Histone H2B.V demarcates strategic regions in the *Trypanosoma cruzi* genome, associates with a bromodomain factor and affects parasite differentiation and host cell invasion

Juliana Nunes Rosón[abc], Marcela de Oliveira Vitarelli[ab], Héllida Marina Costa-Silva[ab], Kamille Schmitt Pereira[de], David da Silva Pires[ab], Leticia de Sousa Lopes[ab], Barbara Cordeiro[ab], Amelie J. Kraus[fg], Karin Navarro Tozzi Cruz[ab], Simone Guedes Calderano[ab], Stenio Perdigão Fragoso[de], T. Nicolai Siegel[fg], Maria Carolina Elias[ab], Julia Pinheiro Chagas da Cunha[ab].

[a]Laboratory of Cell Cycle, Butantan Institute, São Paulo, Brazil.
[b]Center of Toxins, Immune Response and Cell Signaling (CeTICS), Butantan Institute, São Paulo, Brazil.
[c]Department of Microbiology, Immunology and Parasitology, Escola Paulista de Medicina – UNIFESP, São Paulo, Brazil.
[d]Department of Bioprocesses and Biotechnology, Universidade Federal do Paraná, Curitiba, Paraná, Brazil.
[e] Laboratory of Molecular and Systems Biology of Trypanosomatids, Carlos Chagas Institute, FIOCRUZ, Curitiba, PR, Brazil.
[f] Division of Experimental Parasitology, Faculty of Veterinary Medicine, Ludwig-Maximilians-Universität in Munich, Planneg-Martinsried, Germany
[g] Biomedical Center, Division of Physiological Chemistry, Faculty of Medicine, Ludwig-Maximilians-Universitäat in Munch, Planegg-Martinsried, Germany

Short title: **Role of H2B.V in the *T. cruzi* genome, differentiation and infection**

#Address correspondence to Julia Pinheiro Chagas da Cunha, julia.cunha@butantan.gov.br.

Key words: Histone, pulldown, epigenetics, chromatin, *Trypanosoma cruzi*, ChIP-seq.

Abstract

Histone variants play a crucial role in chromatin structure organization and gene expression. Trypanosomatids have an unusual H2B variant (H2B.V) that is known to dimerize with the variant H2A.Z generating unstable nucleosomes. Previously, we found that H2B.V protein is enriched in nonreplicative life forms of *Trypanosoma cruzi,* suggesting that this variant may contribute to the differences in chromatin structure and global transcription rates observed among parasite life forms. Here, we performed the first genome-wide profiling of histone localization in *T. cruzi* using replicative and nonreplicative life forms, and we found that H2B.V was preferentially located at the edges of divergent switch regions, which encompass putative transcriptional start regions; at some tDNA loci; and between the conserved and disrupted genome compartments, mainly at trans-sialidase, mucin and MASP genes. Remarkably, the chromatin of nonreplicative forms was depleted of H2B.V-enriched peaks in comparison to replicative forms. Interactome assays indicated that H2B.V associated specifically with H2A.Z, bromodomain factor 2, nucleolar proteins and a histone chaperone, among others. Parasites expressing reduced H2B.V levels were associated with higher rates of parasite differentiation and mammalian cell infectivity. Taken together, H2B.V demarcates critical genomic regions and associates with regulatory chromatin proteins, suggesting a scenario wherein local chromatin structures associated with parasite differentiation and invasion are regulated during the parasite life cycle.

Author Summary

Trypanosomatids have to adapt to different environmental conditions, changing their morphology, gene expression and metabolism. These organisms have many unique features in terms of gene expression regulation. The genomic organization includes polycistronic regions with the absence of well-defined transcription start sites. In *T. brucei*, histone variants mark the start and ending sites of transcription; however, little is known about whether these proteins change their genome location, expression levels and interactors along life forms and what the impact is of these changes on parasite differentiation and infection. In *T. cruzi,* the causative agent of Chagas disease, we previously found that the histone variant of H2B is enriched in

nonreplicative and infective forms, suggesting that this variant may contribute to the differences in chromatin structure and global transcription rates observed among these life forms. Here, we aimed to go one step further and performed the first histone ChIP-seq analysis in *T. cruzi*, in which we found that H2B.V was enriched at divergent strand switch regions, some tDNA loci and other critical genomic regions associated with *T. cruzi* genome compartments. We found that H2B.V interacts with a bromodomain factor, suggesting an intricate network involving chromatin acetylation around H2B.V enriched sites. Moreover, parasites expressing reduced H2B.V levels were associated with higher rates of differentiation and mammalian cell infectivity.

Introduction

Chromatin is formed from the interactions among DNA, RNAs and proteins. Histones are responsible for establishing the folded chromatin structure, presented as nucleosomes, where each one contains two dimers of H2A-H2B and one tetramer of H3-H4. Changes in chromatin conformation caused by histone posttranslational modifications (PTMs) and variant histone deposition can affect interactions in chromatin structure and gene expression [1,2]. Histone variants, aside from canonical histones, differ in primary structure and may be located in specific genomic regions and tissues. For example, CENP-A is a histone variant of histone H3 that is specifically located at centromeres [3]. H2A.Z is present in diverse organisms, destabilizes nucleosome structure and is implicated in transcription activation [4,5]. Few H2B variants have been identified in eukaryotes, including TH2B, which is involved in the cell cycle of germinative mouse male cells [6]; a H2B.Z involved in gene expression in apicomplexans [7], and a H2B.V in trypanosomatids [8], which will be further explored below.

Trypanosomatids are phylogenetically located at one of the deepest branches in eukaryote lineages and include protozoan parasites that cause important human diseases. These organisms have unique characteristics that are mainly related to gene expression and genome structure. Protein-coding genes are organized in long polycistronic transcription units (PTUs) with preferential transcription initiation from interpolycistronic regions located at divergent strand

switch regions (dSSRs) and termination at interpolycistronic regions located at convergent strand switch regions (cSSRs) [9–11].

Strikingly, trypanosomatids contain variants for all core histones, including a H2B.V [12–14]. In *T. brucei*, histone variants have been shown to play a major role in defining transcription start regions (TSRs) and transcription termination regions (TTRs). H2A.Z and H2B.V dimerize and are frequently located at TSRs together with BDF3, H4K10ac and H3K4me3, forming an active chromatin region for RNA Pol II transcription [12]. In this organism, the TSRs located at dSSRs are GT-rich and are more prone to promoting H2B.V-H2A. Z deposition and transcription initiation [15]. H3.V and H4.V are frequently located at TTRs together with enrichment of J bases [12,16].

The genome of *Trypanosoma cruzi*, the etiological agent of Chagas disease, was first sequenced by second-generation sequencing strategies in 2005 [17] and then assembled into 41 *in silico* chromosomes [18]. Compared to the genomes of other trypanosomatids, such as those of *T. brucei* and Leishmania spp., the *T. cruzi* genome contains more repetitive sequences, mainly composed of multigenic family members (such as trans-sialidases, mucins, MASP, GP63, RHS and DGF-1), which harbor almost 30% of their genome [19], making genome assembly challenging. To overcome this problem, the genomes of two *T. cruzi* strains (TCC and Dm28c) were recently sequenced into long reads generated by third-generation sequencing technologies [20], allowing an accurate estimation of gene abundance, length, and distribution of repetitive sequences. One striking observation was that the *T. cruzi* genome is composed of two compartments that differ in gene composition and have opposite GC contents. The disrupted genome compartment contains the majority of nonsyntenic genes of trans-sialidases, mucins, and MASPs that are important virulence factors [21], while the conserved compartment contains the syntenic genes of conserved and hypothetical conserved genes.

Similar to other trypanosomatids, *T. cruzi* is able to adapt and survive in different environmental conditions, requiring fast alterations in morphology, metabolism and gene expression [22–24]. Changes in nuclear and chromatin structure together with a global change in transcription rate follow the differentiation of replicative and noninfective forms (epimastigote

and amastigote) to nonreplicative and infective forms (tissue culture-derived trypomastigote and metacyclic trypomastigote (TCT and MT, respectively) [25,26]. Furthermore, the nucleosome landscape of epimastigotes and TCTs differs mainly at dSSRs [27]. In addition to these alterations, parasite histones are differentially modified by methylation, acetylation and phosphorylation during the cell cycle and differentiation [28–34].

Previously, we found that H2B.V is differentially abundant in chromatin extracts from replicative and nonreplicative *T. cruzi* forms [35], suggesting that this variant might contribute to the differences in chromatin structure and global transcription rates observed among these life forms [25]. As *T. brucei* H2B.V is deposited at TSRs [12], we hypothesized that *T. cruzi* H2B.V might play a critical role in parasite life forms by modulating chromatin structure and gene expression. Thus, here we aimed to explore this hypothesis by evaluating H2B.V interactors, and by searching for H2B.V genomic location and parasite phenotypic changes along the cell and life cycle using CRISPR-tagged and knockout parasites. H2B.V was shown to be enriched at dSSRs and other critical genomic regions. Moreover, parasites expressing reduced H2B.V levels were associated with higher rates of differentiation and mammalian cell infectivity.

Results

H2B.V demarcates *T. cruzi* divergent switch strand regions, some tDNA loci and genome compartments.

H2B.V is present as a single-copy gene at chromosome 27 in the *T. cruzi* CL Brener genome assembly. Thus, to evaluate the genomic location of H2B.V, we generated parasites expressing tagged H2B.V at the C-terminus with 3 x myc peptides by CRISPR-Cas9 methodology (S1A Fig). The genomic edition of the H2B.V locus was confirmed by western blotting and immunofluorescence assay (S1B Fig). Due to the lack of antibodies against endogenous H2B.V, it was not possible to compare the expression levels of wild-type versus myc-tagged H2B.V.

To identify the genomic regions associated with nucleosomes harboring H2B.V, the chromatin of myc-tagged epimastigotes and TCTs was digested with micrococcal nuclease

(MNase) and sonicated followed by chromatin immunoprecipitation (ChIP) using anti-myc and anti-histone H3 antibodies (as a control for the nucleosome distribution along genome). Furthermore, the input for all ChIP samples and an additional control sample of an untagged epimastigote cell line (immunoprecipitated with an anti-myc antibody) were also analyzed. To improve the data analysis and biological conclusions, the reads were mapped against two *T. cruzi* genome assemblies (the Esmeraldo-like haplotype of the CL Brener strain and against the TCC strain), and the results obtained for each were compared throughout this study. The first corresponds to the strain used for ChIP experiments, the genome of which was sequenced by second-generation sequencing strategies [17], and the second harbors 99.7% identity to the CL Brener genome and was recently sequenced by PacBio into long reads [20]. By mapping the reads to these two assemblies, we could evaluate whether any bias related to genome sequencing and assembly quality could interfere with the interpretation of our results. Approximately 2 million reads per replicate per ChIP-seq experiment were sequenced, generating approximately 85% and 90% overall alignment (S2A Fig) in the CL Brener and TCC assembly, respectively.

Visual inspection of H2B.V enrichment (Fig 1A) indicated that this variant was deposited along the edges of dSSRs, including, in some cases, the first few coding DNA sequences (CDSs) from the polycistronic regions (Fig 1A and S3A). In accordance, the summary plot of the normalized ratio of H2B.V (ChIP/input) enrichment clearly indicated that H2B.V was preferentially enriched in the upstream region of polycistrons (Fig 1B) in both the CL Brener (Fig 1B) and TCC assembly (S3B Fig). Through H2B.V peak enrichment data, we observed that H2B.V was deposited over large regions of approximately 5 kb in width (Figs 1C and 2SC). dSSRs, but not cSSRs, were demarcated by a peak at each edge, and no specific histone H3 enrichment was found at these regions (Fig 1C). Very little enrichment at cSSR was associated with the existence of tDNAs, as will be discussed below.

We used a peak calling algorithm to faithfully identify and compare peaks among life forms and genome features (S2B-D Figs, S2 and S3 Tables). Peaks were obtained for each replicate separately, but only the overlapping peak set was used for further analysis (S2B-D Figs). From the 265 peaks found in epimastigotes (fold change >=4, Poisson p-value over input required

= 1.00e-04), 91.3% were located at dSSR, and only 8.7% were found at non-SSR in the CL Brener assembly (Fig 1D and S2 Table). A higher enrichment of H2B.V at dSSR (76%) over non-SSR (24%) was also found in the TCC assembly (S3C Fig).

Although the great majority of H2B.V peaks were located within a dSSR, not all dSSRs contained H2B.V enrichment (S4 Fig). Specifically, 38% and 68% of dSSRs did not have any H2B.V peak (considering a fold change (ChIP/input) of 2) in the CL Brener and TCC assembly, respectively. However, these dSSRs usually flank monocistrons (67% and 60% in the CL Brener and TCC assembly, respectively); small (fewer than 4 CDSs) polycistrons (7.5% and 12% in CL Brener at TCC, respectively); snoDNA, rDNA or tDNA (21% in the TCC assembly). In the CL Brener assembly, we additionally noticed that 20% of the dSSRs that did not harbor the H2B.V peak were located close to a gap assembly region. In short, only 5% and 6% of dSSRs located between two protein coding polycistronic regions (with more than 4 CDSs) lacked H2B.V enrichment.

Among the H2B.V peaks located at non-SSRs, we found that they were closely associated with tDNA genes (25% and 5% in CL Brener and TCC, respectively), snoRNA genes (4% in CL Brener and 6% in TCC), and, more strikingly, between the disrupted and conserved genome compartments (46% -11 out of 23, in the CL Brener assembly) (Figs 1D, 2A, S3C, S4A). In the TCC assembly, 45% of the non-SSR H2B.V peaks were between disrupted and conserved compartments (S3C and S4B Figs).

To further explore this phenomenon, we evaluated the enrichment of H2B.V among multigenic family members composing the disrupted genome compartments (trans-sialidases, MASP, and mucins) and those that could be part of both conserved and disrupted compartments (GP63, RHS, and DGF-1). Heatmaps of H2B.V ChIP data indicated that members of disrupted families were more enriched in H2B.V (Fig 2B). Hierarchical clustering of all multigenic family members showed that mucins and MASP were preferentially enriched on H2B.V (14 and 15%, respectively, considering each gene class individually) (Figs S4B and C). Interestingly, evaluation of these two gene families in the most recent genome assembly with long reads [20] suggested

197 that they are preferentially located at the first CDSs, which in turn would partially explain the
198 enrichment of H2B.V in these gene families.

199 A considerable number of non-SSR H2B.V peaks were located close to tDNA genes.
200 Thus, we evaluated the enrichment of H2B.V in tDNA loci by deeptools analysis (Fig 2C). H2B.V
201 was enriched either at upstream or downstream regions of tDNA genes, with no clear association
202 with tDNA anticodon type or adjacent polycistron transcription direction. tDNA genes were
203 present alone or in clusters of 2 - 10 genes totaling 21 loci in the CL Brener Esmeraldo-like
204 haplotype. Most of them were located within a protein-coding polycistron, suggesting that tDNA
205 loci might interfere with RNA Pol II transcription elongation. Of the 10 loci of tDNA located at
206 non-SSRs, seven were associated with a H2B.V peak (fold >2); from the six tDNA loci located
207 at dSSR, all were associated with an H2B.V peak, while 2 out of 4 located at cSSR had an H2B.V
208 peak.

209 Taken together, H2B.V was enriched at dSSRs flanking protein-coding polycistrons, at
210 some tDNA loci, and at regions between the disrupted and conserved genome compartments. In
211 contrast, dSSRs mainly associated with monocistrons and small polycistrons did not have H2B.V
212 enrichment.

213

214 **H2B.V Chip-seq enrichment differs greatly among replicative and nonreplicative**
215 **forms.**

216 Previously, H2B.V was found to be enriched in TCT chromatin when similar masses (in
217 micrograms) of chromatin proteins from both life forms were compared [35]. We confirmed that
218 H2B.V was enriched in TCT whole cell extracts (WCE) when equal numbers of epimastigotes
219 and TCT parasites (in biological quadruplicates) were compared, while no important difference
220 was found for histone H3 (S6 Fig).

221 Intriguingly, fewer sites of H2B.V enrichment were found along the TCT genome when
222 compared with epimastigotes (Figs 1A, S2B and S3A). While 265 H2B.V-enriched peaks were
223 found at epimastigotes, and only 6 peaks were found at TCTs (fold change over the input >=4) in

the CL Brener assembly. Using the same parameters, fewer and smaller (in width, in bp) peaks were found in TCT life forms than in epimastigote forms in the TCC assembly (Figs S2B-C). These findings suggest that the parasite modulates H2B.V enrichment in life forms, as will be discussed below.

H2B.V interacts with a bromodomain factor and nucleolar proteins.

To gain better insights into the role of H2B.V in chromatin, we evaluated its interaction partners in epimastigotes and TCTs by pulldown assays. Therefore, recombinant H2B.V and canonical H2B (as a bait control) were used to obtain specific H2B.V interactors using the WCE of epimastigotes and TCTs. In addition, four control samples (described in detail in the Materials and Methods section) were also analyzed, which included the analysis of both parasite WCE and the recombinant protein extracts upon affinity resin incubation.

Protein eluates were processed for mass spectrometry, and the results were subjected to *in silico* filtering steps (described in Materials and Methods) to obtain a more meaningful protein set of H2B.V interactors (Fig 3A, S4 and S5 Tables). From the final list of 39 interactors, two proteins were present in all pulldown eluates: double RNA binding domain protein 3 (TcCLB.506649.80) and polyadenylate-binding protein (TcCLB.508461.140), which is known to interact selectively and noncovalently with a sequence of adenylyl residues in an RNA molecule and participate in mRNA maturation at the poly(A) tail [36]. Interestingly, H2B.V interacts more with proteins found at TCTs than at epimastigote extracts. Eight proteins were found to interact with H2B.V in epimastigotes, whereas 26 proteins were found to interact with H2B.V in TCTs. Six were common to both, including 2 nucleosome assembly proteins (TcCLB.507963.79 and TcCLB.504839.50) and a hypothetical protein (TcCLB.509761.10) that was recently annotated as histone chaperone Rttp106-like, known in *S. cerevisiae* for being associated with DNA replication and heterochromatin silencing [37]. Interestingly, the latter was not found in canonical H2B pulldowns, suggesting that it might be associated with H2B. V nucleosome assembly.

Among H2B.V and H2B interactors in TCT extracts, we found a high mobility group protein TDP1 (TcCLB.507951.114), which recognizes and links noncanonical DNA structures,

252 such as cruciform DNA and circular mini-DNA, in addition to its involvement in DNA folding
253 [38,39]; a lupus La protein homolog (TcCLB.511367.60), which is an mRNA ligand and
254 participates in mRNA maturation and translation, and stabilization of histone mRNAs during the
255 S phase in humans [40,41], in addition to binding the 3′ poly(U)-rich in nascent RNA polymerase
256 III transcripts participating in its correct folding and maturation in *T. brucei* [42]; a
257 retrotransposon hot spot (RHS) protein (TcCLB.506113.60); and tousled-like kinase II
258 (TcCLB.510597.9). The latter has enzymatic activity and is involved in several biological
259 processes, such as DNA replication and S-phase progression, repair and H3S10 phosphorylation
260 [43,44].

261 One of the most interesting findings was the presence of 3 nucleolar proteins specifically
262 in H2B.V-TCT pulldowns: nucleolar protein 56 (TcCLB.511573.58), fibrillarin
263 (TcCLB.510105.50), nucleolar RNA-binding protein (TcCLB.511573.58). In addition, two other
264 hypothetical proteins (TcCLB.508409.180 and TcCLB.503829.80) were also detected, which
265 were previously annotated as proteins of the nuclear pore and nuclear envelope, respectively
266 [45,46]. Among H2B.V-specific interactors, we identified protein bromodomain factor 2 (BDF2)
267 (TcCLB.506553.20), an epigenetic factor that recognizes histone acetylation [47,48]. In *T. cruzi*,
268 BDF2 has already been shown to interact with histone H4 acetylated residues (K10 and K14),
269 showing increased levels after exposure to UV in epimastigote forms and likely being involved
270 in the response to DNA damage [49].

271 The H2B.V and BDF2 interaction was validated by reverse pulldown assays using
272 recombinant BDF2-6xHis-HA and WCE of H2B.V-myc-tagged parasites (epimastigotes and
273 TCTs) (Fig 3 B). In contrast to what was observed in H2B.V pulldowns, here the BDF2 interacted
274 with H2B.V in both life forms. In addition, the BDF2 interaction with H2B.V seemed to be
275 specific and not a spurious histone interaction, as histone H3 was not eluted from the BDF2
276 pulldown.

277 It is worth mentioning that besides H2B.V and H2B, we only detected H4 peptides in our
278 pulldown assays. Here, the proteomics protocol was not optimized for histone identification,
279 which is often overdigested by trypsin due to high amounts of lysine and arginine residues. In *T.*

brucei, H2B.V dimerizes with the variant H2A.Z [50] and is preferentially detected at dSSRs. To verify whether *T. cruzi* H2B.V also dimerized with H2A.Z, we cloned and expressed the recombinant H2A.Z (TcCLB.511323.40) fused to a maltose binding protein (MBP) and incubated it with the 6xHis-tagged H2B.V recombinant (Fig 3C). Upon elution with maltose, both H2A.Z-MBP (~60 kDa) and H2B.V-6xHis (~16.5 kDa) were eluted, indicating that H2A.Z-H2B.V also interacted in *T. cruzi*. This *in vitro* interaction was further confirmed by Western blot analysis using polyclonal antibodies against H2A.Z (S7 Fig).

H2B.V is essential but H2B.V heterozygous knockout (H2B.V-HtzKO) epimastigotes do not display alterations in growth, replication or global transcription levels.

To further understand the biological role of histone H2B.V in *T. cruzi*, we generated H2B.V knockout parasites by homologous recombination. Therefore, constructs containing neomycin resistance genes flanked by sequences from the 5' and 3' UTRs of the H2B.V gene (NEO cassette) were generated (S8A Fig) and used to obtain parasites that had lost one H2B.V allele and gained resistance to neomycin. The correct insertion of the neomycin cassette into the H2B.V locus was confirmed by PCR using specific primers (S8B Fig). Many attempts to delete the second H2B.V allele and generate double knockout (or homozygous knockout) parasites using a similar strategy described above (but with a cassette containing the hygromycin resistance gene – described in Materials and Methods) were performed without success. Thus, these results suggested that the H2B.V gene must be essential for *T. cruzi*, similar to *T. brucei* [50]. Thus, all phenotypic analyses described below were performed using two clones (cl 2 and 4) isolated from the transfected parasite population of HtzKO.

First, we confirmed that H2B.V transcription levels were decreased in HtzKO parasites by qPCR (Fig 4A) and by quantitative proteomics assays (iBAQ values) using basic WCE (S8C Fig). H2B.V-HtzKO cl2 and cl4 had, on average, 4 times less H2B.V protein than wild-type cells (unpaired t-test, p-value < 0.05). In accordance, the levels of histone H4 and all other histones did

not change significantly in H2B.V-HtzKO mice. Then, we evaluated whether the lower levels of H2B.V in H2B.V-HtzKO parasites interfered with growth and cell cycle progression. No statistically significant differences were found among H2B.V-HtzKO clones and wild-type parasites when growth and cell cycle phases were evaluated (Figs 4B, S9A-C).

As H2B.V was enriched at putative TSRs, we asked whether H2B. V-HtzKO parasites would show a decrease in global transcription by evaluating EU incorporation. Again, no significant global differences were found among clones and wild-type parasites (S9D Fig).

The reduced H2B.V levels might result in a more stable chromatin structure once nucleosomes containing H2A.Z-H2B.V are more unstable than canonical nucleosomes [12]; thus, we evaluated whether H2B.V-HtzKO parasites would have global changes in chromatin structure by evaluating the amount of active chromatin extracted by the FAIRE approach [51]. We observed a decreasing trend (not statistically significant) in the levels of active chromatin on H2B.V-HtzKO when compared to wild-type parasites (S9E Fig).

Since we evaluated global effects on transcription and active chromatin levels, we could not rule out that specific genomic regions could be affected in H2B.V-HtzKO parasites. Future transcriptomic and sequencing analyses from the data shown in Figures S9D-E could clarify this issue.

Changes in H2B.V levels can affect metacyclogenesis and infection of mammalian cells.

To assess whether the decrease in H2B.V levels in H2B.V-HtzKO parasites affect the differentiation of epimastigotes into metacyclic forms, we performed a metacyclogenesis assay evaluating both the presence of fully differentiated metacyclics and their intermediate forms (based on kinetoplast morphology and position relative to the nucleus as previously described [24]. Labeling of the metacyclic membrane markers GP90 and GP82- was also used to discriminate differentiated parasites [52].

In the stationary growth phase, H2B.V-HtzKOs (cl2) had approximately 60% more intermediate parasite forms than wild-type parasites (S9F Fig), suggesting that changes in H2B.V levels might facilitate the differentiation of epimastigotes into metacyclic trypomastigotes. Furthermore, in the 96-h supernatant after the induction of metacyclogenesis, almost 3 times more trypomastigote metacyclics were found in H2B.V-HtzKO when compared to wild-type parasites (Fig 4C). This supernatant was also enriched in nonmetacyclic parasites (classified as "others", which included epimastigote and intermediate forms), suggesting that changes in H2B.V levels promoted loss of adhesion to substrates.

We also evaluated whether the ability to infect mammalian cells would be affected in H2B.V-HtzKOs TCTs. Surprisingly, we found that cl2 and cl4 infected approximately twice as many cells as wild type (Fig 4D). Taken together, these data suggested that decreasing H2B.V levels might interfere with parasite differentiation and infection of mammalian cells.

Discussion

H2B has few variants described in eukaryotes, but trypanosomatids have a H2B.V that has been shown to dimerize with H2A.Z [50] and to be predominantly located at dSSRs [12]. Here, we investigated the genomic location, interaction partners, and phenotypic changes in single knockout H2B.V parasites in both replicative (epimastigote) and nonreplicative (TCT) life forms. To our knowledge, our work is not just the first histone ChIP-seq analysis performed in *T. cruzi* but also the first to compare, from a genome-wide perspective, the differences in replicative and nonreplicative forms in trypanosomatids, shedding light on epigenetic changes in these organisms, as discussed above.

We found that H2B.V was preferentially located at *T. cruzi* dSSR edges extending ~5 kb and included the first few CDSs at a polycistron. Importantly, H2B.V enrichment was also found at a few non-SSRs, which were preferentially close to tDNAs and, strikingly, between the disrupted and conserved genome compartments, with enrichment mainly in mucin and trans-sialidase genes. Moreover, the great majority of dSSRs flanking polycistrons containing protein-

coding genes showed an enrichment of H2B.V. In contrast, dSSRs flanking monocistrons and short polycistrons (less than 4 CDSs) did not contain a significant enrichment of H2B.V. Future studies should clarify why these dSSRs are not enriched in H2B.V and whether its absence has any transcriptional consequences for the flanked polycistron.

It is well known that global transcription levels are decreased in TCTs in relation to epimastigote forms [25], and similar findings have been found in *T. brucei* [53,54]. Recently, we observed that dSSRs in TCTs have more nucleosomes, which are less dynamic than those from epimastigote forms [27]. Here, we detect that H2B.V is predominantly located at dSSRs of epimastigotes but very few H2B.V enrichment peaks were found on TCTs' genome. Although, the H2B.V protein abundance is higher on TCTs, the absence of clear H2B.V enrichment peaks in this life form was not expected. We hypothesized that either H2B.V was spread along the TCT genome or weakly bound to TCT chromatin in comparison to epimastigotes. Nucleosomes harboring H2B.V-H2A.Z are less stable than canonical nucleosomes [12], and their absence could (partially) explain why dSSRs of TCTs were more occupied by nucleosomes than epimastigotes [27]. We speculate that the absence of histone variants would result in a more stable chromatin structure around dSSRs that, in turn, could hamper RNA Pol II binding, likely explaining the decreased global levels of transcription in this life form [25].

One question that remains to be answered concerns what induces the differential H2B.V enrichment on *T. cruzi* chromatin among life forms. One explanation could be the presence of specific H2B.V/H2A. Z PTMs for each life form. However, we detected no statistically significant difference between H2B.V PTMs in epimastigotes and TCTs, and we found changes in acetylation levels at H2A.Z peptide ^{41}GKGKGKGKGKR^{51} between epimastigotes and TCTs [31]. Another possibility concerns the expression and half-life of H2B.V and the protein complexes involved in its deposition. The deposition of histone variants in chromatin is usually independent of DNA replication [55], but how it is achieved is still not fully understood. In humans, the mammalian homolog SWC2 (YL1) is related to H2A.Z deposition [56]. In *T. brucei*, the GT-rich promoters and H4 acetylation target H2A.Z deposition [15,57]; however, no protein complex was associated with this function. In our pulldown assays, we detected one histone chaperone

(TcCLB.509761.10-histone chaperone Rttp106-like) that interacted specifically with H2B.V, providing a promising candidate for H2B.V deposition. It remains unclear whether this chaperone indeed has a role and whether its levels are differentially expressed throughout the parasite lifecycle affecting H2B.V deposition.

The interactome data highlighted the presence of pore and nuclear envelope proteins (TcCLB.503829.80 and TcCLB.508409.180), suggesting a preferential location of H2B.V in the nuclear periphery. Furthermore, H2B.V interacted with important nucleolar proteins, which might suggest that H2B.V deposition could also influence RNA pol I activity in addition to RNA pol II. Here, we observed an accumulation of H2B.V along rDNA genes (S5C Fig); however, rDNA assessment is always challenging due to its very repetitive nature. In the TCC genome assembly, for example, 249 rDNA genes were distributed over 11 contigs.

In *T. cruzi*, BDF2 was located in the nucleus at all life cycle stages and was shown to interact with acetylated histone H4 K10 and K14 residues [49]. Here, we found that BDF2 interacted with H2B.V, suggesting a chromatin environment in which acetylated lysines were present. Bromodomain proteins have an important role in chromatin function, since their bromine domain participates in biological processes such as DNA replication, transcription, DNA repair and silencing [58–60]. In *T. brucei*, the dSSR is enriched on BDF3 [12], possibly interacting with the many acetylated histones found at dSSRs [57]. Histone acetylation, histone variant deposition and mRNA levels are intrinsically connected in *T. brucei*. Loss of TSS-H4 acetylation reduces H2A.Z deposition in TSS to shift the RNA initiation site, while H2A.Z acetylation is directly associated with increased global mRNA levels [57]. It remains to be investigated whether BDF2 is important to integrate this scenario in *T. cruzi*. Nevertheless, we have previously found multiple acetylations at H2B.V and H2A.Z in *T. cruzi*, the acetylation levels of which change during metacyclogenesis [31]. It is worth noting that in *T. brucei*, BDF2 has been shown to be associated with H2A.Z N-terminal hyperacetylation [61].

The peculiar genome location of H2B.V together with its interaction partners suggested that H2B.V might be associated with important regulatory functions in *T. cruzi*. Single knockouts for H2B.V showed no important effects on proliferation, the cell cycle or global transcription

rates in epimastigote forms, suggesting that i. these processes are independent of H2B.V regulation; ii. other undescribed protein might fulfil the H2B.V function; or iii. the reduced level of H2B.V in HtzKO clones were insufficient to induce critical changes in the abovementioned processes. We believe that the latter hypothesis is more feasible, as we failed to obtain a double knockout parasite, which suggests that H2B.V is essential for cell viability. Moreover, we observed critical effects on metacyclogenesis and mammalian cell infection in H2BV-HtzKO parasites. These results raise the question of how changes in H2B.V abundance would interfere with these phenomena considering the trypanosome's posttranscriptional regulation scenario. In trypanosomes, the 3D nuclear structure and compartmentalization play a crucial role in the spatial organization of splicing and transcription [62]; moreover, parasites that have lost H4.V and H3.V show profound changes in nuclear architecture [63]. In accordance, we found H2B.V enriched at the border of conserved and disrupted genome compartments. The latter is composed of important virulence factors (trans-sialidase, MASP, and mucin genes) that are mainly expressed in metacyclics forms [22]. In addition, lower levels (although not statistically significant) of active chromatin were found in HtzKO-H2B.V parasites when compared with wild-type parasites, suggesting changes in the global chromatin structure. Thus, it is tempting to proposed that H2B.V may mark the transition between these two compartments influencing the *T. cruzi* nuclear architecture and gene expression of these virulence factors.

T. cruzi H2B.V may also harbor moonlight functions affecting cell invasion and differentiation. H2B.V-HtzKO parasites easily lost adhesion to substrates and differentiated almost 3 times more into metacyclics than wild-type parasites. Loss of adhesion to a substrate is critical for epimastigote-to-metacyclic differentiation [64]. However, we could not determine the direct connection between H2B.V and the differentiation/infection capacity, and the changes in histone levels and infectivity are not unprecedented. Leishmania cell lines overexpressing histone H1 have lower infectivity both *in vitro* and in vivo [65–67]. More recently, Leishmania histone H3 was shown to interact with human nuclear histones as part of their nucleosomes [68], which reinforces evidence showing that parasite infection may change the host epigenome [69].

Intriguingly, histones are identified on the secretome of *T. cruzi* [70]. Whether H2B.V have any other role in parasite infection needs to be further explored.

Our data indicate 23 putative new TSRs at non-SSRs (CL Brener Esmeraldo-like haplotype), in which at least 7 were associated with the presence of a tDNA gene inside a polycistron of CDSs. tRNAs are transcribed by RNA Polymerase III and may interfere with RNA Polymerase II transcription/elongation when located near a CDS [12,71–73]. This interference may have special consequences considering the polycistronic transcription scenario in trypanosomatids. In *T. brucei*, an enrichment of H2A.Z was shown downstream of tDNA loci, likely creating a new TSR [12]. Here, we found a more complex scenario: for 3 tDNA loci located at non-SSRs, no H2B.V enrichment was found, suggesting that the absence of a permissive chromatin structure for transcription initiation may negatively interfere with the transcription of the downstream CDSs. If this is correct, it will indicate an interesting alternative to regulate transcription inside the polycistron.

As transcription initiation by RNA pol II in trypanosomatids does not occur on well-defined focused promoters [15], we envisage that these parasites may take advantage of alternative ways to regulate gene expression throughout their life cycle stage by strategically combining the deposition of variant histones such as H2B.V and the location of tDNA genes and nucleosomes in their genome. In addition, the finding that BDF2 interacts with H2B.V may indicate the existence of a complex scenario of histone PTMs at dSSRs that should be explored in the future to highlight further epigenetic modulators, which could be additionally modulated in life forms.

Methods

Parasites, metacyclogenesis, growth curves and mammalian cell invasion. *T. cruzi* epimastigotes (Y and CL Brener strains) were cultured at 28°C in LIT medium supplemented with 10% fetal bovine serum (FBS - Vitrocell), glucose 0.4%, hemin 0.1 µM and penicillin-G 59 mg/L as previously described (Camargo, 1964). H2B.V-HtzKO (cl 2 and 4- Y strain), H2B.V-

myc tagged (CL Brener strain), H2B.V_ab (cl2 and 4- Y strain) and H2B.V-over (Y strain) epimastigote forms were maintained in the abovementioned medium supplemented with 500 µg/mL G418 (Gibco) and 500 µg/mL puromycin and the last two lineages with blasticidin 10 µg/mL. For growth curves, epimastigotes were diluted to 5×10^6 cells/mL and monitored for four days. Cell density was counted in the Z2 Coulter Particle Count and Size Analyzer (Beckman Coulter) using a 100-µm filter. TCT forms (Y and CL Brener strains) were obtained from the supernatant of infected LLCMK2 cells after 1 week of infection (1:40 – cell:parasites) according to [74]. Cells were maintained in DMEM (Gibco) containing $NaHCO_3$ 3.7 g/L, penicillin G 0.059 g/L, streptomycin 0.133 g/L and FBS 10% at 37°C with 5% CO2. For mammalian cell invasion assays, after 1 h of infection (1:40, cell:parasites), cells were fixed with 4% paraformaldehyde, stained with DAPI and visualized by Olympus IX81 fluorescence microscopy. To evaluate epimastigote-to-trypomastigote metacyclic differentiation, the metacyclogenesis protocol described by [75] was followed by evaluating the TAU 3AAG culture supernatant upon 96-144 h of nutritional stress. Intermediate forms were classified based on kinetoplast and nucleus position, as shown in [24]. Antibodies against GP90 and GP82 were used to facilitate visualization of metacyclic parasites. Parasites were counted in technical triplicates from each biological triplicate.

Generation of H2B.V-HtzKO parasites. All primers sequences are described in Table S1. The regions upstream and downstream of the H2B.V gene (TcCLB.506779.150) were cloned from the genomic DNA of the *T. cruzi* Y strain into the recombinant plasmids pTc2KO-neo and pTc2KO-hyg [76]. The upstream region of the H2B.V gene (434 bp) was amplified by PCR using the primers H2B.V_KpnI (forward) and H2B.V_SalI (reverse) (fragment 5'flank_H2B.V). Simultaneously, the 507-bp fragment from the intergenic region downstream of the H2B.V gene was amplified by the primers H2B.V_BamHI (forward) and H2B.V_XbaI (reverse) (fragment 3'flank_H2B.V). The recombinant plasmids pTc2KO-H2B.V-neo and pTc2KO-H2B.V-hyg were purified, and the "NEO cassette" (2,671 bp) and "HYG cassette" (2.971 bp) were amplified by PCR using the primers H2B.V_KpnI (forward) and H2B.V_XbaI (reverse) (S8 Fig). Parasite transfection and selection were performed by homologous recombination of the NEO cassette,

and parasites resistant to G418 were confirmed by PCR using the primers NEO_F and NEO_R; H2B_EXT_FOR and H2B_EXT_REV, NEO Out R and NEO Out F (S8 Fig). The neomycin-resistant parasites were electroporated with the "HYG cassette" (5'FLANK-HYG-3'FLANK) to generate the H2B.V homozygous knockout, which would be resistant to both G418 and hygromycin B (at 500 µg/mL). Clones were obtained by serial dilution by FACS sorting.

Generation of H2B.V-myc parasites. All primer sequences are described in Table S1. The CRISPR-Cas9 protocol was based on [77]. Donor DNA and sgRNA were amplified by PCR using high-fidelity Phusion DNA Polymerases (Thermo Fisher Scientific) considering the H2B.V (TcCLB.506779.150) locus. Primers pMOtag forward and reverse were used to amplify the donor DNA from the pMOtag-23M plasmid [78], and the final PCR product was composed of 30 bp of the homologous arm (final 30 nucleotides from the H2B.V gene, excluding the stop codon), 3 copies of Myc epitope sequence, and the puromycin resistance gene and 30-bp homology arm (30 nucleotides from the intergenic region adjacent to the cleavage region). The donor DNA was inserted in the 3' region of the H2B.V gene to be expressed at the C-terminal portion of H2B.V protein. Primers "TcH2Bv 3´ UTR sgRNA" and "sg scaffold" were used to amplify sgRNA. PCR products were purified (QIAquick PCR Purification Kit Protocol) and transfected into epimastigotes expressing Cas9 (CL Brener strain). A total of 10^8 epimastigotes were resuspended in 350 µL of transfection buffer (90 mM sodium phosphate, 5 mM potassium chloride, 0.15 mM calcium chloride, 50 mM HEPES, pH 7.2) together with 50 µL of purified DNA (PCR products for donor DNA and sgRNA). The 400-µL final volume was placed in 0.2-cm cuvettes (Bio-Rad) and electroporated in the Bio-Rad Gene pulser with 2 pulses of 500 µF and 450 V. After electroporation, parasites were placed in fresh LIT medium with 10% SFB at 28°C. Then, after 24 h, puromycin was added to the medium at a final concentration of 10 µg/mL. After approximately two weeks, the polyclonal population was selected and then cloned. Epimastigotes were diluted to 1 parasite per mL in LIT/10% SFB containing puromycin and then plated in 96-well plates (200 µL per well). The parasites were incubated at 28°C with 5% CO_2, and monoclonal populations were obtained within approximately 3 weeks.

Cloning and recombinant protein expression. All primer sequences are described in Table S1. The H2B gene (TcCLB.511635.10), BDF2 (TcCLB.506553.20) and H2A.Z (TcCLB.511323.40) from *T. cruzi* (CL Brener strain) were amplified using the following pair of primers (all containing Eco RI and Hind III cleavage sites): H2Bc_F and H2Bc_R; HA_BDF2_Forward and BDF2_Reverse, and H2A.Z_Forward and H2A.Z_Reverse. BDF2 was amplified by fusion with HA from the vector pDEST17, which was kindly provided by Dr. Esteban Serra. The PCR products were purified and cloned first at pJET1/2blunt (Invitrogen), and after SANGER sequencing confirmation, the insert was subcloned either at pET28(a)+ (Novagen) (for H2B and BDF2) or at pMAL-p2x (NEB) (for H2A.Z). Plasmids were transfected into *E. coli* DH5α and/or at BL21 DE3 for recombinant expression as described previously [35]. Briefly, *E. coli* BL21 DE3 transformed either with pET28a (+)-H2B.V [35], pET28a(+)-H2B, pET28a(+)-BDF2 or pMAL-p2x-H2A.Z were inoculated in LB base medium (tryptone 1%, NaCl 1%, yeast extract 0.5%, pH 7) containing kanamycin 50 µg/mL at 37°C for up to 18 h, and recombinant expression was induced with 1 mM IPTG. H2B, H2B.V and BDF2 (His-tag) and H2A.Z (fused with a maltose-binding protein -MBP) purification were performed by affinity chromatography using Ni-NTA agarose (Qiagen) and amylose resin (NEB), respectively, according to the manufacturer's recommendations.

Cell cycle and EU (5-Ethynyl-2'-uridine) assay. Epimastigotes in the exponential growth phase were fixed in 70% ethanol overnight at -20°C and treated with 10 µg/mL RNase A (Thermo Scientific) and 40 µg/mL propidium iodide (Sigma-Aldrich, St. Louis, MO). Cells were analyzed using the Attune® Acoustic Focusing Cytometer (Applied Biosystems). Epimastigotes in the exponential growth phase (~5x10^6 cells/mL) were incubated with EU 10 µg/mL (Life) and fixed in cold 50% ethanol for 20 min, as described in [79]. Cells were analyzed using the Attune® Acoustic Focusing Cytometer (Applied Biosystems). Data from 20,000 events were analyzed using FlowJo v. 10.7.1 software.

Protein extracts. A total of 5×10^8 parasites were used to obtain basic protein extracts [32]. Extracts were quantified using the PierceTM BCA Protein Assay Kit protocol (Thermo Scientific) and stored at -20°C.

Pulldown assays. The pulldown protocol was based on the principle of immobilization of recombinant protein using Ni-NTA agarose resin (Qiagen). The experiments were performed in biological triplicates and designed to contain 4 control samples (resin Ni-NTA with i. bacteria extract, ii. Recombinant H2B. V or BDF2, iii. epimastigote extracts, iv. TCT extracts) and 2 experimental extracts (Ni-NTA resin i. epimastigote extracts and recombinant H2B.V or BDF2; ii. TCT extracts and recombinant H2B.V or BDF2). Recombinant protein was first incubated with nickel resins for 30 min under slow stirring at 4°C, followed by a 1-h incubation with parasite basic protein extracts (described above). The resin was washed three times with TBS, and recombinant protein and its interactors were eluted with 50 mM sodium phosphate, 0.3 M NaCl and 290 mM imidazole buffer. One-third of the eluate was reserved for fractionation by SDS-PAGE, and the remainder was reserved for proteomics analysis. The BDF2 eluates were analyzed by western blotting.

Proteomics analysis. Pulldown eluates and parasite extracts (basic protein extracts from H2B.V-HtzKO parasites) were precipitated with 20% TCA and resuspended in 8 M urea, 75 mM NaCl, and 50 mM Tris, pH 8.2. Protein was reduced with 5 mM DTT and alkylated with 14 mM iodoacetamide followed by digestion with trypsin (1:100, w:w) (Promega) as described in [80]. The peptides were resuspended in 0.1% formic acid and injected (5 µl) into a precolumn (Thermo - C18 of 5 µm, 2 cm x 100 µm) coupled to a nano HPLC (NanoLC-1DPlus, Proxeon). The separation was carried out in a capillary precolumn (10 cm x 75 µm containing C18 resins of 3 µm) in a 2-50% gradient of acetonitrile in 0.1% formic acid for 1 h. The eluted peptides were analyzed directly on an Orbitrap spectrometer (LTQ-Orbitrap Velos-Thermo). The 10 most intense ions were selected for fragmentation by CID. All ions were analyzed in positive ionization mode. The data in * raw format were processed using the Andromeda-MaxQuant program [81] with TriTrypDB (*T. cruzi* taxonomy - obtained from http://tritrypdb.org/tritrypdb/). Database

searches were performed using the following parameters: carbamidomethylation of cysteine as a fixed modification; oxidation of methionine, N-terminal acetylation as variable modifications; tolerance MS1 of 6 ppm and MS2 of 0.5 Da, and 1% FDR. The ProteinGroups.txt output was sequentially processed using the Perseus program [81]. Proteins with LFQ intensity values equal to zero were considered absent. Proteins considered by MaxQuant as contaminants, presented in the reverse database and identified only by a modified peptide, were removed. For pulldown analysis, we also removed proteins presented (LFQ value > 0) in only one of the 3 biological replicates; proteins with a ratio of LFQ values from the experimental sample (EpiH2B, TripoH2B, EpiH2BV and TripoH2BV) to the control sample (Control_Epi, Control_TCT) lower than 1.5 (to ensure that eluted protein was enriched in the pulldown assay over the control samples); and common contaminant proteins (ribosomal, cytoskeleton, heat-shock and metabolic proteins). Finally, we only considered proteins that were present in a previous chromatin study [35] and those with *T. brucei* protein orthologs located in the nucleus/chromatin according to TrypTag. For histone quantitation on H2B.V-HtzKOs, the iBAQ values for all detected histones were considered 100%.

ChIP-seq. ChIP-seq experiments were performed as described in [15] with a few modifications. Epimastigote and TCT H2B.V-myc-tagged cells ($1x10^8$) were cross-linked with 1% formaldehyde for 20 min at RT and quenched with 2 M glycine followed by washes with cold TDB buffer (5 mM KCl, 80 mM NaCl, 1 mM $MgSO_4$, 20 mM Na_2HPO_4, 2 mM NaH_2PO_4, and 20 mM glucose (pH 7.4)). The permeabilization buffer and NP-S buffer described in [15] were substituted for lysis buffer (1 mM potassium L-glutamate, 250 mM sucrose, 2.5 mM $CaCl_2$, 1 mM PMSF) [35]. Upon crosslinking, cells were resuspended in 1 mL lysis buffer, centrifuged, and resuspended in lysis buffer containing 0.1% Triton X-100 for 15 min at RT. Then, the cells were pelleted, washed, and incubated with 75 U of Mnase (Sigma Aldrich, #N3755) at 25°C for 10 min. After the addition of 10 mM EDTA to block digestion, the supernatant was collected and washed with lysis buffer with 0.1% SDS. The pellet was sonicated in a Covaris S220 (1 min, 10% duty factor, 200 cycles per burst). Sheared DNA was centrifuged (10,000 x g for 10 min at 4°C). Fifty microliters of Dynabeads protein G (Thermo Fisher) was resuspended in PBS-Tween

(0.02%) containing 10 µg of purified anti-Myc antibody (Helmholtz Zentrum München, Monoclonal Antibody Core Facility) and incubated with slow rotation at 4°C overnight. Antibody-coupled beads were incubated at 4°C overnight with slow rotation with the MNase supernatant obtained above, washed eight times with cold RIPA buffer (50 mM HEPES-KOH pH 7.5, 500 mM LiCl, 1 mM EDTA, 1% NP-40, 0.7% Na-deoxycholate), washed one time with TE buffer containing 50 mM NaCl and eluted with 50 mM Tris-HCl pH 8.0, 10 mM EDTA, 1% SDS at 65°C for 30 min. The crosslinking of ChIP and input samples was reversed with 300 mM NaCl (at 65°C for 9 h) and treated with RNase A and proteinase K as described. After DNA purification, ChIP and input DNA samples were used to construct an Illumina library using TruSeq adapters according to [15]. The libraries were sent for Illumina NextSeq sequencing with 75-bp paired-end sequencing at the Core Unit Systems Medicine, University of Würzburg.

ChIP-seq analysis. Quality filtering and adapter trimming of the Illumina sequencing reads were performed with fastp version 0.20.0 [60]. Reads with more than 5 N bases were discarded, as were those with more than 40% of their bases with Phred quality values below 15 (< Q15). All nucleotides from the 5' or 3' ends of each read with quality inferior to 5 (< Q5) were removed. Since these data were paired-end, we activated the correction algorithm: for size overlaps of at least 30 nucleotides (accepting 5 mismatches), a base is corrected if it is ultralow quality (< Q15), while the corresponding base at the mate read is high quality (> Q30). After the application of all these filters, reads shorter than 15 base pairs were removed. Approximately 94% of the reads passed the described filters and were used for downstream analysis. Quality control was performed with FastQC version 0.11.8 [61]. The local mapping of the filtered reads against the genome of the CL Brener Esmeraldo-like strain (release 32) and against the TCC strain (release 44) from TriTrypDB was performed with bowtie2 version 2.3.5.1 [62], with parameters more restrictive than the preset option: very-sensitive-local parameters (-D 25 -R 4 -N 1 -L 19 -i S,1,0.40 --nceil L,0,0.15). Coverage plots were generated using COVERnant v.0.3.2 (https://github.com/konrad/COVERnant) and visualized using IGV (http://software.broadinstitute.org/software/igv/). COVERnant ratios were obtained by pairwise analysis of each ChIP and input sample. For the identification of genomic regions

enriched in H2B.V, the bam files were analyzed using the findPeaks (-sytle histone), getDiffPeaks (-style histone) and mergePeaks (-d given [default] = maximum distance to merge) commands from HOMER [64] with default options. Peaks were obtained by the findPeaks command considering a fold (-f) enrichment of 2 or 4 over the corresponding input sample. To analyze histone enrichment at specific genomic regions, genomic coordinates of each feature were obtained from an in-house customized GFF file. Summary plots and heatmaps were obtained using the computeMatrix (with scale-regions and skipZeros options) and plotHeatmap (with hierarchical clustering) functions from deepTools2 [82,83]. The GFF file from *T. cruzi* (available at https://tritrypdb.org/) was customized in-house to contemplate the polycistrons, dSSRs and cSSRs.

WB and immunofluorescence (IFA). WB and IFA were performed as described with antibodies, and the dilutions used were as follows: anti-Myc (Cell Signaling) 1:3000; anti-HA (Cell Signaling) 1:3000, anti-H3 (Abcam) 1:10000, and anti-H2A. Z (polyclonal – kindly provided by Dr. Nicolai Siegel), anti-His Tag (Cell Signaling) 1:3000; anti-GAPDH 1:4000 (polyclonal) [84]. For IFA of myc-tagged parasites, after fixation with 4% paraformaldehyde and permeabilization with Triton X-100, an overnight incubation with anti-Myc (Cell Signaling) antibody 1:3000 in 1% PBS/BSA at 4°C followed by secondary antibody conjugated to Alexa Fluor 555 (Thermo Fisher) at 1:500 in PBS/BSA 1% was performed. When mentioned, IFA using anti-GP90 and anti-GP82 1:1000 (kindly provided by Nobuko Yoshida) was performed as described previously [85]. Slides were further mounted with Vectashield plus DAPI (Vector laboratories) and visualized at 100 X magnification in an inverted OLYMPUS microscope model IX81 with Z axis motorization. Images were acquired using OLYMPUS CELL R version software 3.2.

Quantitative PCR. TRIzol Reagent (Invitrogen) was used to isolate total RNA from *T. cruzi* epimastigotes in exponential growth phase. Next, 10 µg from each total RNA sample was subjected to DNAse I (Sigma) treatment to remove genomic DNA contamination. Then, 1 µg of purified RNA was used for cDNA synthesis with a Super Script™ Reverse Transcriptase Kit

(Invitrogen) following the manufacturer's recommendations. Quantitative real-time PCRs were performed using H2B.V_qPCR_F and H2B.V_qPCR_R as the target genes, and GAPDH_Tcruzi_qPCR_Fw and GAPDH_Tcruzi_qPCR_Rv were used as endogenous control genes (Table S1). For each reaction, 5 µL of 2X Power SYBR Green PCR Master Mix (Applied Biosystems), 2 ng cDNA, and 300 nM H2B.V primer or 100 nM GAPDH primer were used. All reactions were carried out in triplicate in a 96-well plate. The plates were run on a StepOnePlus™ Real Time PCR System (Applied Biosystems). The relative quantification of H2B.V transcripts was calculated by the $2^{-\Delta Ct}$ method [86].

Faire assay. The FAIRE samples were prepared as described in [87] with some modifications. The $2x10^8$ epimastigotes of wild type, H2B.V HtzKO cl2 and cl4 were fixed with 37% formaldehyde and directly added to LIT medium to a final concentration of 1% for 5 minutes at RT. The formaldehyde was quenched with 2.5 M glycine to a final concentration of 125 mM. Then, the parasite pellets were resuspended in 2 mL of cold TELT buffer (50 mM Tris-HCl pH 8.0, 62.5 mM EDTA, 2.5 M LiCl, 4% Triton X-100) and sonicated in a Tommy Ultrasonic Disruptor UD-201 apparatus with an output of 4 and duty of 30 for 10 cycles of 30 seconds with 1-minute intervals. To prepare input control DNA, one-fourth (500 µL) of each sample was incubated with 5 µL of proteinase K for 1 h at 55°C, and the cross-linking was reversed by overnight incubation at 65°C. After that, the DNA was extracted with phenol:chloroform:isoamyl alcohol solution and precipitated with 3 M sodium acetate (pH 5.2) and 95% ethanol. The input control DNA obtained was quantified using a NanoDrop (Thermo Fisher). To verify the sonication efficiency, 500 ng of input DNA control was run on a 1% agarose gel. To prepare FAIRE DNA, half of the fixed cell lysate (1 mL) was used. DNA was extracted as described above; however, protein removal by proteinase K and cross-linking reversal were performed after DNA purification. Then, DNA was purified with a MinElute PCR Purification Kit (Qiagen) following the manufacturer's recommendations. To assess the DNA yield, the total quantity of control DNA or FAIRE DNA (in ng, obtained by Nanodrop quantitation) was divided by the volume of cell lysate used for control DNA or FAIRE DNA obtention (in µL), respectively.

687 Considering the control DNA yield as 100%, the retrieval ratio of FAIRE DNA for each sample
688 was calculated.
689

690 ## Acknowledgments

691 We thank Ivan Novaski Avino and Ismael Feitosa Lima for technical assistance and Alex Ranieri
692 Lima for important inputs on the data and bioinformatic analysis. We thank Esteban Serra for the
693 BDF2 plasmid, Roberto Docampo for the pMOtag23M plasmid, and Nobuko Yoshida for
694 antibodies against metacyclic markers (GP90 and GP82). We thank Herbert Guimarães de Sousa
695 Silva for reading this manuscript and providing critical comments. This work was supported by
696 fellowships from FAPESP and by grants (#2017/06104-3, #19/04483-2, #18/15553-9,
697 #16/50050-2, #13/07467-1) from the Sao Paulo Research Foundation (FAPESP). JNR was
698 supported by a fellowship from CAPES, MO and HCS were supported by fellowships from
699 FAPESP, and BC was supported by fellowships from Fundação Butantan. MCE has a fellowship
700 from the National Council for Scientific and Technological Development (CNPq).
701

702 ## References

703 1. Goldberg AD, Allis CD, Bernstein E. Epigenetics: A Landscape Takes Shape. Cell.
704 2007;128: 635–638. doi:https://doi.org/10.1016/j.cell.2007.02.006

705 2. Henikoff S. Nucleosome destabilization in the epigenetic regulation of gene expression.
706 Nat Rev Genet. 2008;9: 15–26. doi:10.1038/nrg2206

707 3. Sullivan KF, Hechenberger M, Masri K. Human CENP-A contains a histone H3 related
708 histone fold domain that is required for targeting to the centromere. J Cell Biol.
709 1994/11/01. 1994;127: 581–592. doi:10.1083/jcb.127.3.581

710 4. Zlatanova J, Thakar A. H2A.Z: view from the top. Structure. 2008;16: 166–179.
711 doi:10.1016/j.str.2007.12.008

712 5. Santoro SW, Dulac C. Histone variants and cellular plasticity. Trends Genet. 2015;31:
713 516–527. doi:10.1016/j.tig.2015.07.005

714 6. Montellier E, Boussouar F, Rousseaux S, Zhang K, Buchou T, Fenaille F, et al.
715 Chromatin-to-nucleoprotamine transition is controlled by the histone H2B variant
716 TH2B. Genes Dev. 2013;27: 1680–1692. doi:10.1101/gad.220095.113

717 7. Hoeijmakers WAM, Salcedo-Amaya AM, Smits AH, Francoijs K-J, Treeck M,
718 Gilberger T-W, et al. H2A.Z/H2B.Z double-variant nucleosomes inhabit the AT-rich
719 promoter regions of the Plasmodium falciparum genome. Mol Microbiol. 2013;87:
720 1061–1073. doi:10.1111/mmi.12151

721 8. Talbert PB, Ahmad K, Almouzni G, Ausió J, Berger F, Bhalla PL, et al. A unified
722 phylogeny-based nomenclature for histone variants. Epigenetics Chromatin. 2012;5: 7.
723 doi:10.1186/1756-8935-5-7

724 9. Martínez-Calvillo S, Nguyen D, Stuart K, Myler PJ. Transcription initiation and
725 termination on Leishmania major chromosome 3. Eukaryot Cell. 2004;3: 506–517.
726 doi:10.1128/ec.3.2.506-517.2004

727 10. Hekstra DR, Dewell S, Siegel TN, Wang X, Cross GAM. Genome-wide analysis of
728 mRNA abundance in two life-cycle stages of Trypanosoma brucei and identification of
729 splicing and polyadenylation sites . Nucleic Acids Res. 2010;38: 4946–4957.
730 doi:10.1093/nar/gkq237

731 11. Martinez-Calvillo S, Yan S, Nguyen D, Fox M, Stuart K, Myler PJ. Transcription of
732 Leishmania major Friedlin chromosome 1 initiates in both directions within a single
733 region. Mol Cell. 2003;11: 1291–1299.

734 12. Siegel TN, Hekstra DR, Kemp LE, Figueiredo LM, Lowell JE, Fenyo D, et al. Four
735 histone variants mark the boundaries of polycistronic transcription units in Trypanosoma

brucei. Genes Dev. 2009;23: 1063–1076. doi:10.1101/gad.1790409

13. Anderson BA, Wong ILK, Baugh L, Ramasamy G, Myler PJ, Beverley SM. Kinetoplastid-specific histone variant functions are conserved in Leishmania major. Mol Biochem Parasitol. 2013/09/27. 2013;191: 53–57. doi:10.1016/j.molbiopara.2013.09.005

14. Alsford S, Horn D. Trypanosomatid histones. Mol Microbiol. 2004;53: 365–372. doi:10.1111/j.1365-2958.2004.04151.x

15. Wedel C, Forstner KU, Derr R, Siegel TN. GT-rich promoters can drive RNA pol II transcription and deposition of H2A.Z in African trypanosomes. EMBO J. 2017;36: 2581–2594. doi:10.15252/embj.201695323

16. Cliffe LJ, Siegel TN, Marshall M, Cross GAM, Sabatini R. Two thymidine hydroxylases differentially regulate the formation of glucosylated DNA at regions flanking polymerase II polycistronic transcription units throughout the genome of Trypanosoma brucei. Nucleic Acids Res. 2010/03/09. 2010;38: 3923–3935. doi:10.1093/nar/gkq146

17. El-Sayed NM, Myler PJ, Bartholomeu DC, Nilsson D, Aggarwal G, Tran A-N, et al. The Genome Sequence of Trypanosoma cruzi, Etiologic Agent of Chagas Disease. Science (80-). 2005;309: 409–415. doi:10.1126/science.1112631

18. Weatherly DB, Boehlke C, Tarleton RL. Chromosome level assembly of the hybrid Trypanosoma cruzi genome. BMC Genomics. 2009/06/03. 2009;10: 255. doi:10.1186/1471-2164-10-255

19. Pita S, Díaz-Viraqué F, Iraola G, Robello C. The Tritryps Comparative Repeatome: Insights on Repetitive Element Evolution in Trypanosomatid Pathogens. Genome Biol Evol. 2019;11: 546–551. doi:10.1093/gbe/evz017

20. Berná L, Rodríguez M, Chiribao ML, Parodi-Talice A, Pita S, Rijo G, et al. Expanding an expanded genome: long-read sequencing of Trypanosoma

cruzi bioRxiv. 2018; 279174. doi:10.1101/279174

21. De Pablos LM, Osuna A. Multigene Families in Trypanosoma cruzi and Their Role in Infectivity. Maurelli AT, organizador. Infect Immun. 2012;80: 2258 LP – 2264. doi:10.1128/IAI.06225-11

22. Berna L, Chiribao ML, Greif G, Rodriguez M, Alvarez-Valin F, Robello C. Transcriptomic analysis reveals metabolic switches and surface remodeling as key processes for stage transition in Trypanosoma cruzi. PeerJ. 2017/03/14. 2017;5: e3017. doi:10.7717/peerj.3017

23. de Godoy LMF, Marchini FK, Pavoni DP, Rampazzo R de CP, Probst CM, Goldenberg S, et al. Quantitative proteomics of Trypanosoma cruzi during metacyclogenesis. Proteomics. 2012;12: 2694–2703. doi:10.1002/pmic.201200078

24. Goncalves CS, Avila AR, de Souza W, Motta MCM, Cavalcanti DP. Revisiting the Trypanosoma cruzi metacyclogenesis: morphological and ultrastructural analyses during cell differentiation. Parasit Vectors. 2018;11: 83. doi:10.1186/s13071-018-2664-4

25. Elias MC, Marques-Porto R, Freymuller E, Schenkman S. Transcription rate modulation through the Trypanosoma cruzi life cycle occurs in parallel with changes in nuclear organisation. Mol Biochem Parasitol. 2001;112: 79–90.

26. Ferreira LR, Dossin Fde M, Ramos TC, Freymuller E, Schenkman S. Active transcription and ultrastructural changes during Trypanosoma cruzi metacyclogenesis. An Acad Bras Cienc. 2008/03/18. 2008;80: 157–166.

27. Lima ARJ, de Araujo CB, Bispo S, Patané J, Silber AM, Elias MC, et al. Nucleosome landscape reflects phenotypic differences in Trypanosoma cruzi life forms. PLoS Pathog. 2021/01/27. 2021;17: e1009272. doi:10.1371/journal.ppat.1009272

784 28. da Cunha JPC, Nakayasu ES, de Almeida IC, Schenkman S. Post-translational
785 modifications of Trypanosoma cruzi histone H4. Mol Biochem Parasitol. 2006;150:
786 268—277. doi:10.1016/j.molbiopara.2006.08.012

787 29. da Cunha JPC, Nakayasu ES, Elias MC, Pimenta DC, Tellez-Inon MT, Rojas F, et al.
788 Trypanosoma cruzi histone H1 is phosphorylated in a typical cyclin dependent kinase
789 site accordingly to the cell cycle. Mol Biochem Parasitol. 2005;140: 75–86.
790 doi:10.1016/j.molbiopara.2004.12.007

791 30. de Jesus TCL, Nunes VS, Lopes M de C, Martil DE, Iwai LK, Moretti NS, et al.
792 Chromatin Proteomics Reveals Variable Histone Modifications during the Life Cycle of
793 Trypanosoma cruzi. J Proteome Res. 2016;15: 2039–2051.
794 doi:10.1021/acs.jproteome.6b00208

795 31. de Lima LP, Poubel SB, Yuan Z-F, Rosón JN, Vitorino FN de L, Holetz FB, et al.
796 Improvements on the quantitative analysis of Trypanosoma cruzi histone post
797 translational modifications: Study of changes in epigenetic marks through the parasite's
798 metacyclogenesis and life cycle. J Proteomics. 2020;225: 103847.
799 doi:10.1016/j.jprot.2020.103847

800 32. Marques Porto R, Amino R, Elias MCQ, Faria M, Schenkman S. Histone H1 is
801 phosphorylated in non-replicating and infective forms of Trypanosoma cruzi. Mol
802 Biochem Parasitol. 2002;119: 265–271.

803 33. Nardelli SC, da Cunha JPC, Motta MCM, Schenkman S. Distinct acetylation of
804 Trypanosoma cruzi histone H4 during cell cycle, parasite differentiation, and after DNA
805 damage. Chromosoma. 2009;118: 487–499. doi:10.1007/s00412-009-0213-9

806 34. Picchi GFA, Zulkievicz V, Krieger MA, Zanchin NT, Goldenberg S, de Godoy LMF.
807 Post-translational Modifications of Trypanosoma cruzi Canonical and Variant Histones.
808 J Proteome Res. 2017;16: 1167–1179. doi:10.1021/acs.jproteome.6b00655

809 35. Jesus TCL de, Calderano SG, Vitorino FN de L, Llanos RP, Lopes M de C, Araújo CB
810 de, et al. Quantitative Proteomic Analysis of Replicative and Nonreplicative Forms
811 Reveals Important Insights into Chromatin Biology of Trypanosoma cruzi. Mol Cell
812 Proteomics. 2017;16: 23–38. doi:10.1074/MCP.M116.061200

813 36. Bag J, Wu J. Translational control of poly(A)-binding protein expression. Eur J
814 Biochem. 1996;237: 143–152. doi:10.1111/j.1432-1033.1996.0143n.x

815 37. Huang S, Zhou H, Katzmann D, Hochstrasser M, Atanasova E, Zhang Z. Rtt106p is a
816 histone chaperone involved in heterochromatin-mediated silencing. Proc Natl Acad Sci
817 U S A. 2005;102: 13410 LP – 13415. doi:10.1073/pnas.0506176102

818 38. Das BB, Dexheimer TS, Maddali K, Pommier Y. Role of tyrosyl-DNA
819 phosphodiesterase (TDP1) in mitochondria. Proc Natl Acad Sci U S A. 2010/11/01.
820 2010;107: 19790–19795. doi:10.1073/pnas.1009814107

821 39. Caldecott KW. DNA single-strand breaks and neurodegeneration. DNA Repair (Amst).
822 2004;3: 875–882. doi:https://doi.org/10.1016/j.dnarep.2004.04.011

823 40. McLaren RS, Caruccio N, Ross J. Human La protein: a stabilizer of histone mRNA. Mol
824 Cell Biol. 1997;17: 3028–3036. doi:10.1128/mcb.17.6.3028

825 41. Crosio C, Boyl PP, Loreni F, Pierandrei-Amaldi P, Amaldi F. La protein has a positive
826 effect on the translation of TOP mRNAs in vivo. Nucleic Acids Res. 2000;28: 2927–
827 2934. doi:10.1093/nar/28.15.2927

828 42. Shan F, Mei S, Zhang J, Zhang X, Xu C, Liao S, et al. A telomerase subunit homolog La
829 protein from Trypanosoma brucei plays an essential role in ribosomal biogenesis. FEBS
830 J. 2019;286: 3129–3147. doi:https://doi.org/10.1111/febs.14853

831 43. Li Z, Gourguechon S, Wang CC. Tousled-like kinase in a microbial eukaryote regulates
832 spindle assembly and S-phase progression by interacting with Aurora kinase and

chromatin assembly factors. J Cell Sci. 2007;120: 3883–3894. doi:10.1242/jcs.007955

44. Li Z, Umeyama T, Wang CC. The chromosomal passenger complex and a mitotic kinesin interact with the Tousled-like kinase in trypanosomes to regulate mitosis and cytokinesis. PLoS One. 2008;3: e3814. doi:10.1371/journal.pone.0003814

45. Goos C, Dejung M, Janzen CJ, Butter F, Kramer S. The nuclear proteome of Trypanosoma brucei. PLoS One. 2017;12: e0181884. doi:10.1371/journal.pone.0181884

46. Zhou Q, Lee KJ, Kurasawa Y, Hu H, An T, Li Z. Faithful chromosome segregation in Trypanosoma brucei requires a cohort of divergent spindle-associated proteins with distinct functions. Nucleic Acids Res. 2018;46: 8216–8231. doi:10.1093/nar/gky557

47. de la Cruz X, Lois S, Sánchez-Molina S, Martínez-Balbás MA. Do protein motifs read the histone code? BioEssays. 2005;27: 164–175. doi:10.1002/bies.20176

48. Mujtaba S, Zeng L, Zhou M-M. Structure and acetyl-lysine recognition of the bromodomain. Oncogene. 2007;26: 5521–5527. doi:10.1038/sj.onc.1210618

49. Villanova GV, Nardelli SC, Cribb P, Magdaleno A, Silber AM, Motta MCM, et al. Trypanosoma cruzi bromodomain factor 2 (BDF2) binds to acetylated histones and is accumulated after UV irradiation. Int J Parasitol. 2009;39: 665—673. doi:10.1016/j.ijpara.2008.11.013

50. Lowell JE, Kaiser F, Janzen CJ, Cross GAM. Histone H2AZ dimerizes with a novel variant H2B and is enriched at repetitive DNA in Trypanosoma brucei. J Cell Sci. 2005;118: 5721–5730. doi:10.1242/jcs.02688

51. Giresi PG, Kim J, McDaniell RM, Iyer VR, Lieb JD. FAIRE (Formaldehyde-Assisted Isolation of Regulatory Elements) isolates active regulatory elements from human chromatin. Genome Res. 2006/12/21. 2007;17: 877–885. doi:10.1101/gr.5533506

856 52. Cordero EM, Gentil LG, Crisante G, Ramírez JL, Yoshida N, Añez N, et al. Expression
857 of GP82 and GP90 surface glycoprotein genes of Trypanosoma cruzi during in vivo
858 metacyclogenesis in the insect vector Rhodnius prolixus. Acta Trop. 2008;105: 87–91.
859 doi:https://doi.org/10.1016/j.actatropica.2007.08.004

860 53. Pays E, Hanocq-Quertier J, Hanocq F, Van Assel S, Nolan D, Rolin S. Abrupt RNA
861 changes precede the first cell division during the differentiation of Trypanosoma brucei
862 bloodstream forms into procyclic forms in vitro. Mol Biochem Parasitol. 1993;61: 107–
863 114. doi:10.1016/0166-6851(93)90163-r

864 54. Christiano R, Kolev NG, Shi H, Ullu E, Walther TC, Tschudi C. The proteome and
865 transcriptome of the infectious metacyclic form of Trypanosoma brucei define quiescent
866 cells primed for mammalian invasion. Mol Microbiol. 2017/08/04. 2017;106: 74–92.
867 doi:10.1111/mmi.13754

868 55. Henikoff S, Smith MM. Histone variants and epigenetics. Cold Spring Harb Perspect
869 Biol. 2015;7: a019364–a019364. doi:10.1101/cshperspect.a019364

870 56. Latrick CM, Marek M, Ouararhni K, Papin C, Stoll I, Ignatyeva M, et al. Molecular
871 basis and specificity of H2A.Z–H2B recognition and deposition by the histone
872 chaperone YL1. Nat Struct Mol Biol. 2016;23: 309–316. doi:10.1038/nsmb.3189

873 57. Kraus AJ, Vanselow JT, Lamer S, Brink BG, Schlosser A, Siegel TN. Distinct roles for
874 H4 and H2A.Z acetylation in RNA transcription in African trypanosomes. Nat Commun.
875 2020;11: 1498. doi:10.1038/s41467-020-15274-0

876 58. Faivre EJ, McDaniel KF, Albert DH, Mantena SR, Plotnik JP, Wilcox D, et al. Selective
877 inhibition of the BD2 bromodomain of BET proteins in prostate cancer. Nature.
878 2020;578: 306–310. doi:10.1038/s41586-020-1930-8

879 59. Gilan O, Rioja I, Knezevic K, Bell MJ, Yeung MM, Harker NR, et al. Selective targeting

of BD1 and BD2 of the BET proteins in cancer and immuno-inflammation. Science (80-). 2020. doi:10.1126/science.aaz8455

60. Zeng L, Zhou MM. Bromodomain: an acetyl-lysine binding domain. FEBS Lett. 2002;513: 124–128.

61. Yang X, Wu X, Zhang J, Zhang X, Xu C, Liao S, et al. Recognition of hyperacetylated N-terminus of H2AZ by TbBDF2 from Trypanosoma brucei. Biochem J. 2017;474: 3817–3830. doi:10.1042/BCJ20170619

62. Faria J, Luzak V, Müller LSM, Brink BG, Hutchinson S, Glover L, et al. Spatial integration of transcription and splicing in a dedicated compartment sustains monogenic antigen expression in African trypanosomes. Nat Microbiol. 2021/01/13. 2021. doi:10.1038/s41564-020-00833-4

63. Müller LSM, Cosentino RO, Förstner KU, Guizetti J, Wedel C, Kaplan N, et al. Genome organization and DNA accessibility control antigenic variation in trypanosomes. Nature. 2018;563: 121–125. doi:10.1038/s41586-018-0619-8

64. Bonaldo MC, Souto-Padron T, de Souza W, Goldenberg S. Cell-substrate adhesion during Trypanosoma cruzi differentiation. J Cell Biol. 1988/04/01. 1988;106: 1349–1358. doi:10.1083/jcb.106.4.1349

65. Papageorgiou FT, Soteriadou KP. Expression of a novel Leishmania gene encoding a histone H1-like protein in Leishmania major modulates parasite infectivity in vitro. Infect Immun. 2002;70: 6976–6986. doi:10.1128/iai.70.12.6976-6986.2002

66. Smirlis D, Bisti SN, Xingi E, Konidou G, Thiakaki M, Soteriadou KP. Leishmania histone H1 overexpression delays parasite cell-cycle progression, parasite differentiation and reduces Leishmania infectivity in vivo. Mol Microbiol. 2006;60: 1457–1473. doi:https://doi.org/10.1111/j.1365-2958.2006.05205.x

904 67. Moreno J, Nieto J, Masina S, Cañavate C, Cruz I, Chicharro C, et al. Immunization with
905 H1, HASPB1 and MML Leishmania proteins in a vaccine trial against experimental
906 canine leishmaniasis. Vaccine. 2007;25: 5290–5300. doi:10.1016/j.vaccine.2007.05.010

907 68. Dacher M, Tachiwana H, Horikoshi N, Kujirai T, Taguchi H, Kimura H, et al.
908 Incorporation and influence of Leishmania histone H3 in chromatin. Nucleic Acids Res.
909 2019;47: 11637–11648. doi:10.1093/nar/gkz1040

910 69. Robert McMaster W, Morrison CJ, Kobor MS. Epigenetics: A New Model for
911 Intracellular Parasite-Host Cell Regulation. Trends Parasitol. 2016;32: 515—521.
912 doi:10.1016/j.pt.2016.04.002

913 70. Bayer-Santos E, Aguilar-Bonavides C, Rodrigues SP, Cordero EM, Marques AF,
914 Varela-Ramirez A, et al. Proteomic Analysis of Trypanosoma cruzi Secretome:
915 Characterization of Two Populations of Extracellular Vesicles and Soluble Proteins. J
916 Proteome Res. 2013;12: 883–897. doi:10.1021/pr300947g

917 71. Wang Q, Nowak CM, Korde A, Oh DH, Dassanayake M, Donze D. Compromised RNA
918 polymerase III complex assembly leads to local alterations of intergenic RNA
919 polymerase II transcription in Saccharomyces cerevisiae. BMC Biol. 2014/10/29.
920 2014;12: 89. doi:10.1186/s12915-014-0089-x

921 72. Oler AJ, Alla RK, Roberts DN, Wong A, Hollenhorst PC, Chandler KJ, et al. Human
922 RNA polymerase III transcriptomes and relationships to Pol II promoter chromatin and
923 enhancer-binding factors. Nat Struct Mol Biol. 2010;17: 620–628.
924 doi:10.1038/nsmb.1801

925 73. Gerber A, Ito K, Chu C-S, Roeder RG. Induced RPB1 depletion reveals a direct gene-
926 specific control of RNA Polymerase III function by RNA Polymerase II. bioRxiv. 2019;
927 764605. doi:10.1101/764605

928 74. Nogueira N, Cohn Z. Trypanosoma cruzi: mechanism of entry and intracellular fate in
929 mammalian cells. J Exp Med. 1976;143: 1402–1420. doi:10.1084/jem.143.6.1402

930 75. Contreras VT, Salles JM, Thomas N, Morel CM, Goldenberg S. In vitro differentiation
931 of Trypanosoma cruzi under chemically defined conditions. Mol Biochem Parasitol.
932 1985;16: 315–327. doi:https://doi.org/10.1016/0166-6851(85)90073-8

933 76. Pavani RS, da Silva MS, Fernandes CAH, Morini FS, Araujo CB, Fontes MR de M, et
934 al. Replication Protein A Presents Canonical Functions and Is Also Involved in the
935 Differentiation Capacity of Trypanosoma cruzi. PLoS Negl Trop Dis. 2016;10:
936 e0005181. Recuperado: https://doi.org/10.1371/journal.pntd.0005181

937 77. Beneke T, Madden R, Makin L, Valli J, Sunter J, Gluenz E. A CRISPR Cas9 high-
938 throughput genome editing toolkit for kinetoplastids. R Soc open Sci. 2017;4: 170095.
939 doi:10.1098/rsos.170095

940 78. Lander N, Li Z-H, Niyogi S, Docampo R. CRISPR/Cas9-Induced Disruption of
941 Paraflagellar Rod Protein 1 and 2 Genes in Trypanosoma cruzi Reveals Their Role in
942 Flagellar Attachment. Sibley LD, organizador. MBio. 2015;6. doi:10.1128/mBio.01012-
943 15

944 79. Ramos TCP, Nunes VS, Nardelli SC, dos Santos Pascoalino B, Moretti NS, Rocha AA,
945 et al. Expression of non-acetylatable lysines 10 and 14 of histone H4 impairs
946 transcription and replication in Trypanosoma cruzi. Mol Biochem Parasitol. 2015;204:
947 1–10. doi:10.1016/j.molbiopara.2015.11.001

948 80. Villen J, Gygi SP. The SCX/IMAC enrichment approach for global phosphorylation
949 analysis by mass spectrometry. Nat Protoc. 2008;3: 1630–1638.
950 doi:10.1038/nprot.2008.150

951 81. Tyanova S, Temu T, Sinitcyn P, Carlson A, Hein MY, Geiger T, et al. The Perseus

computational platform for comprehensive analysis of (prote)omics data. Nat Methods. 2016;13: 731–740. doi:10.1038/nmeth.3901

82. Ramírez F, Ryan DP, Grüning B, Bhardwaj V, Kilpert F, Richter AS, et al. deepTools2: a next generation web server for deep-sequencing data analysis. Nucleic Acids Res. 2016/04/13. 2016;44: W160–W165. doi:10.1093/nar/gkw257

83. Ramírez F, Dündar F, Diehl S, Grüning BA, Manke T. deepTools: a flexible platform for exploring deep-sequencing data. Nucleic Acids Res. 2014;42: W187-91. doi:10.1093/nar/gku365

84. Pariona-Llanos R, Pavani RS, Reis M, Noël V, Silber AM, Armelin HA, et al. Glyceraldehyde 3-Phosphate Dehydrogenase-Telomere Association Correlates with Redox Status in Trypanosoma cruzi. PLoS One. 2015;10: e0120896.

85. Rodrigues JPF, Sant\textquoterightana GHT, Juliano MA, Yoshida N. Inhibition of Host Cell Lysosome Spreading by Trypanosoma cruzi Metacyclic Stage-Specific Surface Molecule gp90 Downregulates Parasite Invasion. Adams JH, organizador. Infect Immun. 2017;85. doi:10.1128/IAI.00302-17

86. Livak KJ, Schmittgen TD. Analysis of relative gene expression data using real-time quantitative PCR and the 2(-Delta Delta C(T)) Method. Methods. 2001;25: 402–408. doi:10.1006/meth.2001.1262

87. Simon JM, Giresi PG, Davis IJ, Lieb JD. Using formaldehyde-assisted isolation of regulatory elements (FAIRE) to isolate active regulatory DNA. Nat Protoc. 2012;7: 256–267. doi:10.1038/nprot.2011.444

Legends

Figure 1. H2B.V is enriched at dSSRs of epimastigote forms. A. IGV snapshot of whole chr 6S of the CL Brener Esmeraldo-like haplotype using the wig files from the ChIP H2B.V/input and ChIP H3/input ratios obtained by COVERnant v.0.3.2. Note that H2B.V, but not H3, is enriched at dSSRs. Blue bar arrows indicate the transcription direction in each polycistron. Genes in the same polycistron are stained with the same color. dSSRs, purple bars; cSSRs, yellow bars. Red bars represent H2B.V -peaks (fold equal to 4 over the input, Poisson p-value over input required = 1.00e-04) obtained by HOMER in the epimastigote form. Summary plot obtained by deepTools for H2B and H3 (ChIP/input) enrichment at polycistrons (B), dSSRs and cSSRs (C). Two kilobases upstream and downstream of the abovementioned regions were also analyzed. All genomic features were automatically scaled as indicated (Start-End). D. Distribution of H2B.V peaks (Fold 4) on all 41 chromosomes of the CL BrenerCL Brener- Esmeraldo-like haplotype.

Figure 2. H2B.V enrichment is also found at the border of conserved and disrupted genome compartments and around tDNA loci. A. IGV snapshot of a 120-kb region from chr 4S highlighting H2B.V enrichment around tDNA loci and between conserved and disrupted genome compartments. Wig files from the ChIP H2B.V/input and ChIP H3/input were obtained by COVERnant. Blue bar arrows indicate the transcription direction in each polycistron. Genes in the same polycistron are stained with the same color. Black and red bars represent tDNA loci and H2B.V -peaks (fold equal to 4 over the input, Poisson p-value over input required = 1.00e-04) obtained by HOMER in epimastigote form. The conserved and disrupted compartments are represented by green and orange bars, respectively. B. Heatmaps of multigenic family members showing ratios of ChIP H2B.V/input and ChIP H3/input in two epimastigote replicates. Note an enrichment (red) of H2B.V at MASP, mucin and TS genes. C. Summary plot obtained by deepTools of the normalized (ChIP/input) H2B.V reads at tDNA loci and the adjacent 2 kb upstream and downstream regions. The tDNA locus was automatically scaled as indicated (first (S) and last (E) nucleotides of each locus). Normalized data were classified into 3 hierarchical clusters (dark blue – 13 genes, light blue – 11 genes and yellow -31 genes) based on the H2B.V enrichment pattern.

Figure 3. H2B.V *in vitro* interactors. A. Venn diagram showing the number of common and specific interactors of H2B.V and H2B using epimastigote and TCT extracts. The total number of eluted proteins in each pulldown is shown between parentheses. Some relevant proteins are highlighted. B. BDF2 pulldown assays. Recombinant BDF2 tagged with HA and 6xHis was incubated with NTA-Ni resins with or without H2B.V-myc-tagged parasite extracts (epimastigotes or TCTs). Eluates were fractionated by 15% SDS-PAGE, and protein interactors were revealed by WB with anti-HA (against rBDF2), anti-myc (against H2B. V-myc tagged), and anti-H3 (as a chromatin control). C. H2A.Z interacts with H2B.V *in vitro*. Recombinant H2A.Z-MBP and recombinant H2B.V-6xHis were incubated together or separately with amylose resin, known to specifically interact with MBP. Eluates were fractionated by 15% SDS-PAGE and stained with Coomassie. H2A.Z-MBP is approximately 60 kDa, and H2B.V-6xHis is 16.5 kDa. The * indicates a contaminant.

Figure 4. Phenotypic evaluation of H2B.V-HtzKO parasites. A. H2B.V relative expression levels were evaluated by qPCR in wild-type and H2B.V-HtzKO (cl 2 and 4) parasites. H2B.V transcript levels were assessed relative to GAPDH levels (ΔCtH2BV – ΔCtGAPDH). One-way ANOVA: * p-value < 0.05. B. Mean growth curves (in log10) for wild-type and H2B.V-HtzKO (cl 2 and 4) parasites. C. Metacyclogenesis assay. The number of metacyclic trypomastigotes, epimastigotes and intermediate forms (herein, classified as other) were counted in 96-h supernatant upon nutritional stress as described in the Materials and Methods. Values were normalized to their respective numbers in wild-type cells. Experiments were performed in biological triplicates. Unpaired T-test: *p < 0.05 and ***p < 0.01 with Bonferroni correction. D. H2B.V-HtzKO parasites are more infective. LLCMK2 cells were infected with TCTs (1:40; cells:parasite). Slides were fixed, and nuclei were labeled with DAPI. The number of infected cells was counted relative to the total cells after 1 h of infection by fluorescence microscopy. Unpaired t-test with Welch's correction *** p < 0.0001.

Supporting information

Supplemental Figures

S1 Fig. H2B.V-myc tagged parasites generated by CRISPR-Cas9.

(A) Schematic representation of CRISPR/Cas9 gene editing of the H2B.V gene (TcChr27-S:430,316 -430,747). The black arrow indicates the cleavage site where a double strand break is caused by the Cas9 enzyme. IGR represents the intergenic region, and HArm represents the homologous arm. Donor DNA was amplified by PCR from the pMOTag23M plasmid using long primers. Long primer sequences are composed of 30 nucleotides corresponding to the homologous arm (5' end of the primer) plus 20 nucleotides complementary to the plasmid (3' end of the primer). The resulting PCR product, called donor DNA, is composed of 30 bp of the homologous arm of the H2B.V gene (in blue); 3 copies of myc sequence (in green); the *T. brucei* tubulin intergenic region (dark gray); the resistance gene to puromycin (in orange); and 30 bp of the homologous arm (in light gray) from the 3' intergenic region (just after the cleavage site). The final edited lócus H2B.V –myc is illustrated at the bottom of the scheme. TcChr27-S:430,316 -430,747. (B) Western blot assays confirm the expression of H2B.V-myc in epimastigotes maintained with puromycin (10 -30 µg/mL). Untransfected parasites were used as a control (ctl). (C) IFA showing the presence of H2B-myc in epimastigote and TCT life forms.

S2 Fig. Mapping coverage and peaks in H2B.V ChIP-seq in CL Brener and TCC assemblies.

(A) Total reads and overall alignment of input and H2B.V- ChIP samples in the CL Brenerr Esmeraldo-like haplotype (release 32) and TCC (release 44) assemblies. (B) H2B.V peaks identified in epimastigotes and TCTs using a peak calling algorithm available in HOMER [27] considering a fold enrichment of 4 (default) (green bars) and 2 (orange bars) and a required Poisson p-value over input = 1.00e-04. Left, number of peaks obtained at each replicate (R) separately. Right panel, number of peaks obtained by a merge peak function available in HOMER. (C) Comparison of peak (fold 4) width (in bp) among life forms and genome mapping. (D) Venn diagrams (available online at https://www.meta-chart.com/) comparing common and different peaks at folds 2 and 4 between life forms.

S3 Fig. Representation of dSSR and cSSR on the TCC strain and signals at CDS polycistrons.

(A) IGV snapshot of H2B.V and H3 enrichment at contig PRFC000010. Note that H2B.V, but not H3, is enriched at dSSR. Blue bar arrows indicate the transcription direction in each polycistron. Genes in the same polycistron are stained with the same color. Red and green bars represent, respectively, H2B.V-peaks (fold 4) obtained by HOMER in epimastigote and TCT life forms. Purple and yellow bars represent dSSRs and cSSRs, respectively. (B) Heatmap plots and k-mean clustering of H2B.V and H3 ChIP-seq signals at CDS polycistrons (deeptools - scale region function) and their 2-kb upstream and downstream regions (hclust = 3), mapped to the TCC assembly. Black regions represent polycistrons that are located at the border of the contigs and therefore have either no upstream or downstream regions. (C) Distribution of H2B.V peaks (fold 4) in the 20 longer contigs (PRFC000001 to PRFC000020) of the TCC assembly.

S4 Fig. **Distribution of enrichment H2B.V peaks in dSSR and multigenic family members.**

(A) IGV snapshot of H2B.V and H3 reads in TcChr23-S showing an enrichment of H2B.V between the conserved (green) and disrupted (orange) genome compartments and two distinct patterns at dSSRs. Blue bar arrows indicate the transcription direction in each polycistron. Genes in the same polycistron are stained with the same color. Red and green bars represent, respectively, H2B.V -peaks (fold 4) obtained by HOMER in epimastigote and TCT life forms. Purple and yellow bars represent dSSRs and cSSRs, respectively. Black and red arrows indicate dSSRs with or without H2B.V enrichment, respectively. (B) Heatmap plots and k-means clustering of H2B.V and H3 ChIP-seq signals in multigenic family members (deeptools - scale region function) and their 2-kb upstream and downstream regions mapped in the CL BrenerCL Brener- Esmeraldo-like and TCC assembly. (C) Distribution of multigenic family members in clusters 1 to 3 described in B (dark blue, light blue and yellow lines in the summary plot). Note that the distribution of these genes in clusters 1 and 2 differs from the expected genome distribution (last bar).

S5 Fig. Examples of enriched H2B.V signal in tDNA, rDNA clusters and dSSR.

IGV snapshot of H2B.V enrichment at tDNA loci (A), rDNA (B) and dSSR (C) in the CL Brener Esmeraldo-like assembly. Blue bars arrows indicate the transcription direction in each polycistron. Genes in the same polycistron are stained with the same color. Red and green bars represent, respectively, H2B.V -peaks (fold 4) obtained by HOMER in epimastigote and TCT life forms. Purple and yellow bars represent dSSRs and cSSRs, respectively. Black bars indicate tDNA or rDNA.

S6 Fig. H2B.V shows more expression in TCT forms.

WCE of TCTs and epimastigotes ($2x10^6$ parasites in quadruplicates) were probed against GAPDH (housekeeping gene), myc (H2B.V) and histone H3. Right, bands were quantified using ImageJ and plotted in Prisma. * t-test (p-value < 0.05).

S7 Fig. H2A.Z interacts with H2B.V *in vitro*.

Recombinant H2A.Z-MBP and recombinant H2B.V-His were incubated together or separately with amylose resin, known to specifically interact with MBP. Eluates were fractionated in a 15% SDS-PAGE and transferred to nitrocellulose membranes. Western blot assay was performed using polyclonal antibodies anti-H2A.Z and anti-His (for H2B.V-HisTag). H2A.Z-MBP is ~60 kDa, and H2B.V-His is ~ 16.5 kDa.

S8 Fig. H2B.V-HtzKO construction and validation.

(A) Diagram of NEO cassette recombination at the H2B.V locus (Chr 27-S) in the *T. cruzi* CL Brener genome highlighting the location of H2B_EXT_FOR and H2B_EXT_REV primers used for amplification of the whole NEO cassette, which includes the 5' and 3' fragments of H2B.V. Lower, the location of primers H2B.V EXT_FOR (forward); Neo F (forward); Neo Out R (reverse); Neo Out F (forward); Neo R (reverse); and H2B.V EXT_REV (reverse) are highlighted. (B) pTc2KO-H2B.V-neo cassette insertion confirmation. Left, the 1% TAE agarose gel showing

the 3045-bp amplicon from the complete NEO cassette recombined at the H2B.V locus (primers H2B_EXT_FOR and H2B_EXT_REV). Right, pTc2KO-H2B.V-neo cassette insertion confirmation in clone 4. A 1% TAE agarose gel of amplificons obtained from PCR using the following pair of primers: 1- H2B.V EXT_FOR / Neo Out R (1052 bp); 2- Neo Out F / H2B.V EXT_REV (1376 bp); 3- H2B.V EXT_FOR / Neo R (1819 bp); 4- Neo F / H2B.V EXT_REV (1966 bp); H2B.V_KpnI_forward / H2B.V_XbaI_reverse (1384 bp) for confirmation of heterozygous knockouts. M(pb)- molecular weight marker in bp (1 Kb Plus Ladder – Invitrogen). (C) Relative abundance of histones in H2B.V-HztKO and wild-type parasites. Total basic extracts from H2B.V-HtzKO and wild-type parasites were evaluated by label-free quantitative proteomics. iBAQ values were obtained from each sample (in biological triplicates), and the relative values were considered. Unpaired t-test (* p-value < 0.05).

S9 Fig. H2B.V-HtzKO phenotypic analysis.

(A). Phase contrast images of H2B.V-HtzKO, and wild-type parasites. (B) Biological replicates of growth curves (in $\log_{10}$) for wild-type and H2B.V-HtzKO (cl 2 and 4) parasites. (C) Percentage of cell cycle phases in H2B.V-HtzKO clones and wild-type parasites. Bars represent the average from biological triplicates. Error bars represent SEM values. (D) Histograms of EU-positive cells of H2B.V-HtzKOs (cl2 and 4), wild-type (orange) and unlabeled parasites (green). The mean and standard variation of the percentage of positive cells were plotted (triplicate values). One-way ANOVA of variance – unpaired-test. (E) Quantitation of the open chromatin of H2B.V-HtzKOs and wild-type parasites obtained after the FAIRE protocol. The retrieval ratio refers to the percentage of open chromatin related to the total DNA content obtained for each sample. (F) Percentage of parasites (epimastigote, intermediate and metacyclic trypomastigotes) in stationary phase culture of H2B.V-HtzKOs and wild-type parasites. Parasites were classified based on the position and morphology of the nucleus and kinetoplast as proposed previously [24]. The metacyclics markers GP90 and GP82 were also used to allow discrimination of life forms.

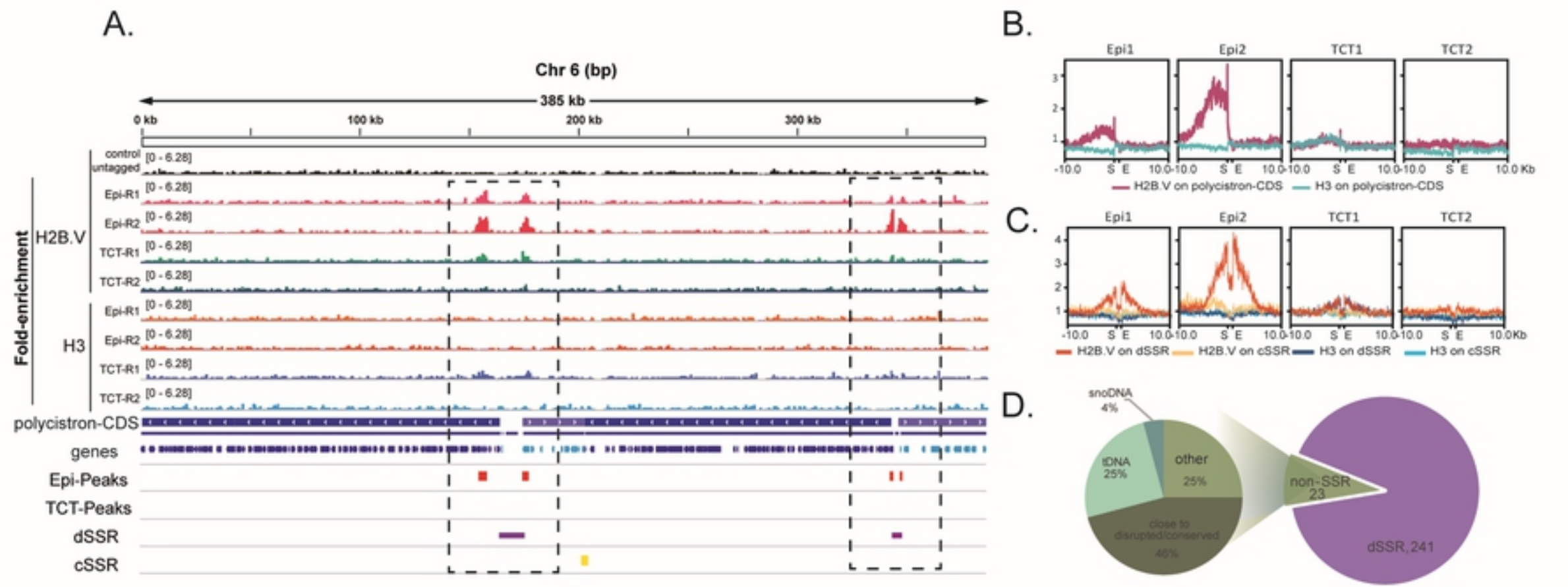
A.
Chr 6 (bp)
385 kb
0 kb
100 kb
200 kb
300 kb
control untagged
[0 - 6.28]
Epi-R1
Epi-R2
TCT-R1
TCT-R2
H2B.V
H3
Fold-enrichment
polycistron-CDS
genes
Epi-Peaks
TCT-Peaks
dSSR
cSSR
B.
Epi1
Epi2
TCT1
TCT2
H2B.V on polycistron-CDS
H3 on polycistron-CDS
C.
H2B.V on dSSR
H2B.V on cSSR
H3 on dSSR
H3 on cSSR
D.
snoDNA 4%
tDNA 25%
other 25%
close to disrupted/conserved 46%
non-SSR 23
dSSR, 241

Fig1

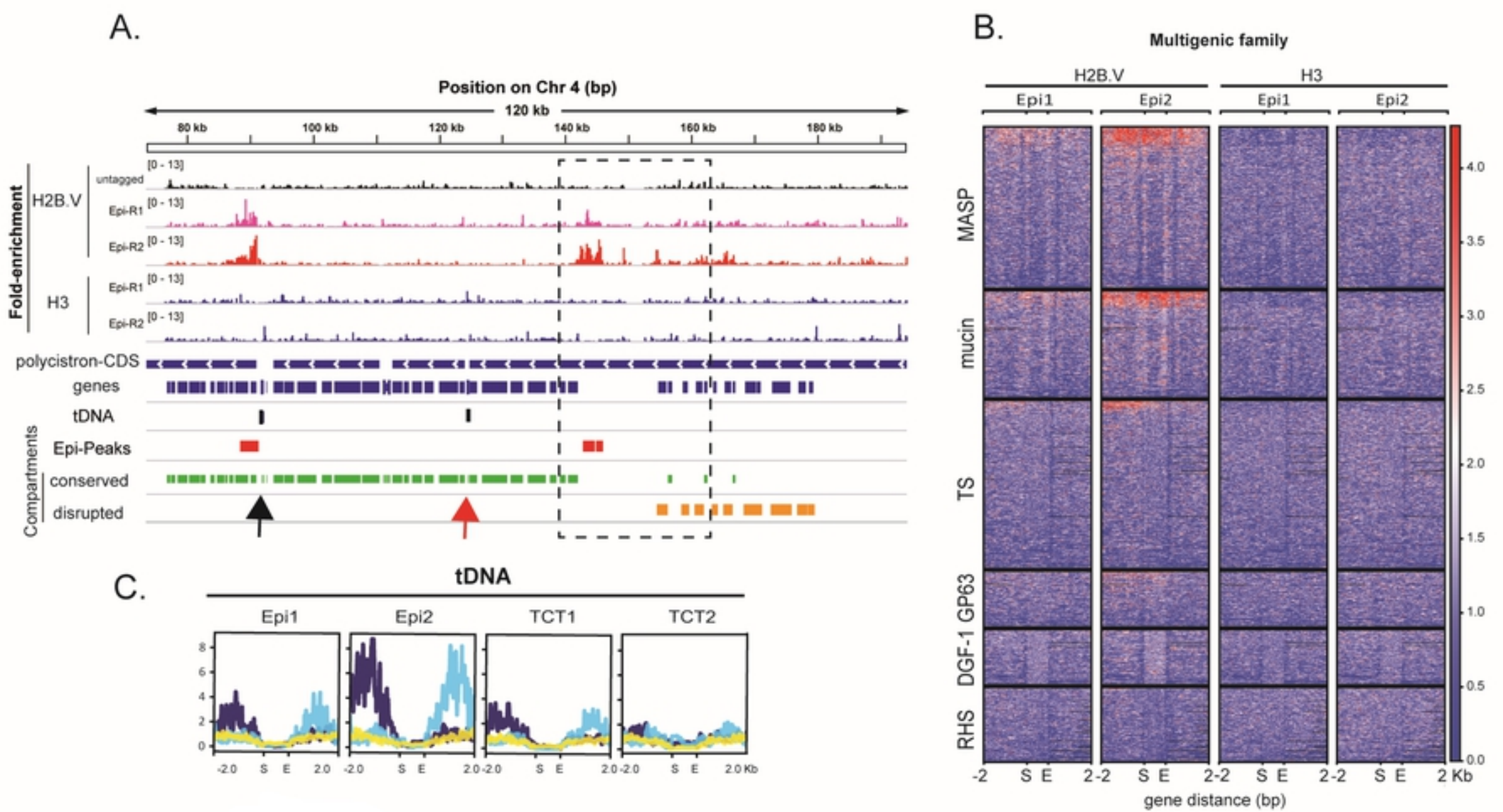
A.
Position on Chr 4 (bp)
120 kb
80 kb
100 kb
120 kb
140 kb
160 kb
180 kb
Fold-enrichment
H2B.V
untagged
Epi-R1
Epi-R2
H3
Epi-R1
Epi-R2
[0 - 13]
polycistron-CDS
genes
tDNA
Epi-Peaks
Compartments
conserved
disrupted
B.
Multigenic family
H2B.V
H3
Epi1
Epi2
Epi1
Epi2
MASP
mucin
TS
GP63
DGF-1
RHS
-2
S E
2
Kb
gene distance (bp)
C.
tDNA
Epi1
Epi2
TCT1
TCT2
-2.0
S E
2.0
Kb

Fig2

A.

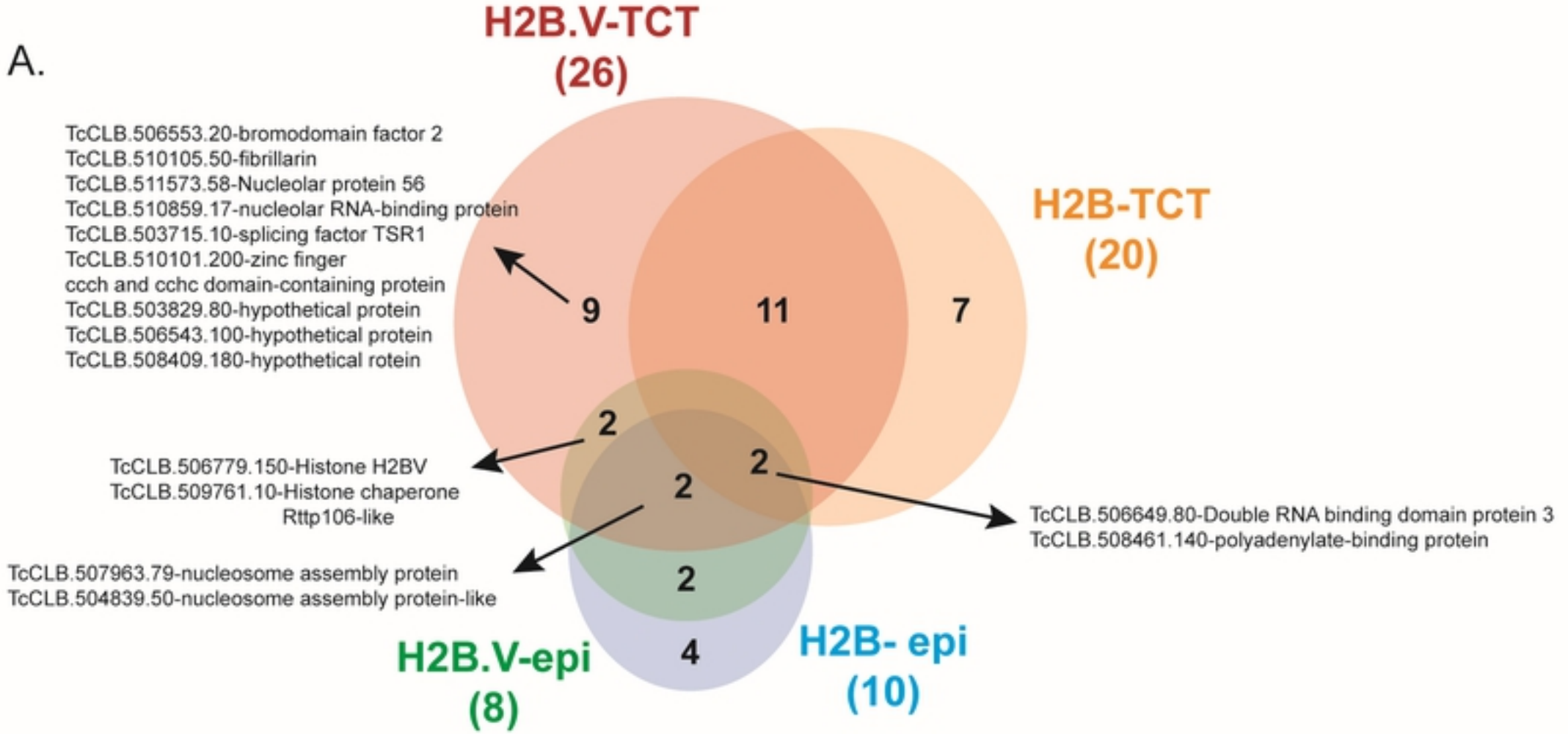
H2B.V-TCT
(26)
H2B-TCT
(20)
H2B.V-epi
(8)
H2B- epi
(10)
TcCLB.506553.20-bromodomain factor 2
TcCLB.510105.50-fibrillarin
TcCLB.511573.58-Nucleolar protein 56
TcCLB.510859.17-nucleolar RNA-binding protein
TcCLB.503715.10-splicing factor TSR1
TcCLB.510101.200-zinc finger
ccch and cchc domain-containing protein
TcCLB.503829.80-hypothetical protein
TcCLB.506543.100-hypothetical protein
TcCLB.508409.180-hypothetical rotein
9
11
7
2
2
2
2
4
TcCLB.506779.150-Histone H2BV
TcCLB.509761.10-Histone chaperone
Rttp106-like
TcCLB.507963.79-nucleosome assembly protein
TcCLB.504839.50-nucleosome assembly protein-like
TcCLB.506649.80-Double RNA binding domain protein 3
TcCLB.508461.140-polyadenylate-binding protein

B.

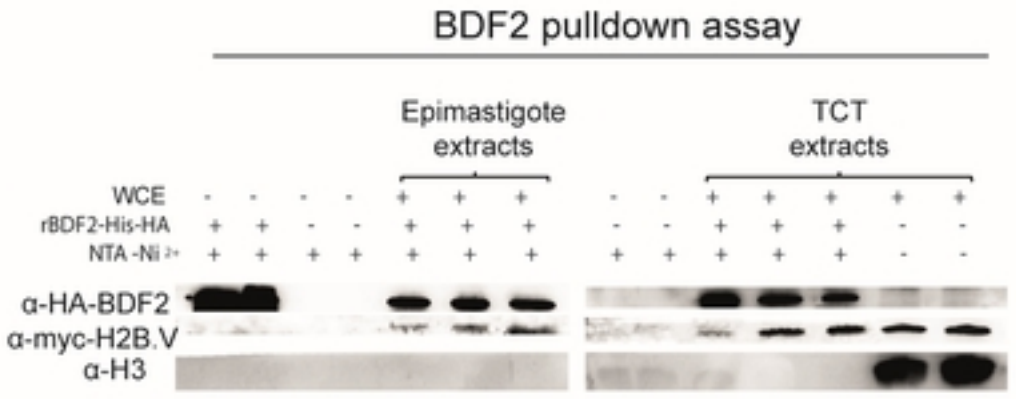
BDF2 pulldown assay
Epimastigote extracts
TCT extracts
WCE
rBDF2-His-HA
NTA -Ni 2+
α-HA-BDF2
α-myc-H2B.V
α-H3

C.

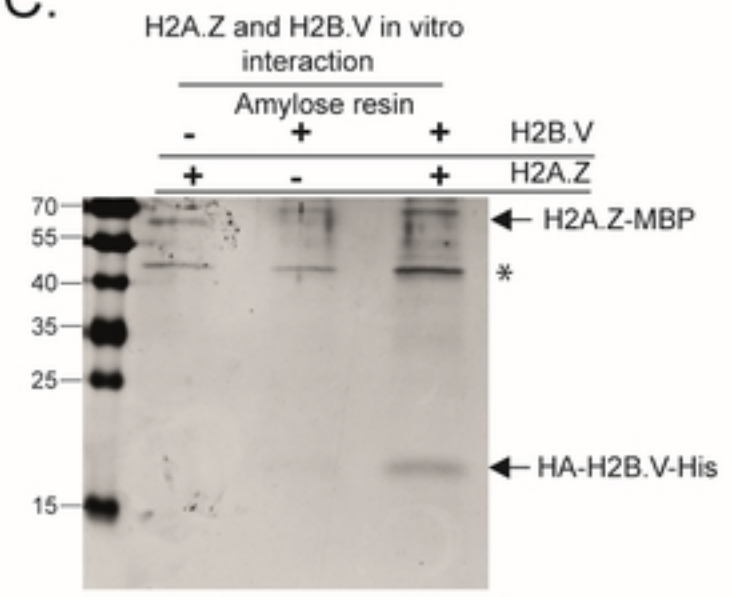
H2A.Z and H2B.V in vitro interaction
Amylose resin
H2B.V
H2A.Z
70
55
40
35
25
15
H2A.Z-MBP
*
HA-H2B.V-His

Fig3

A.

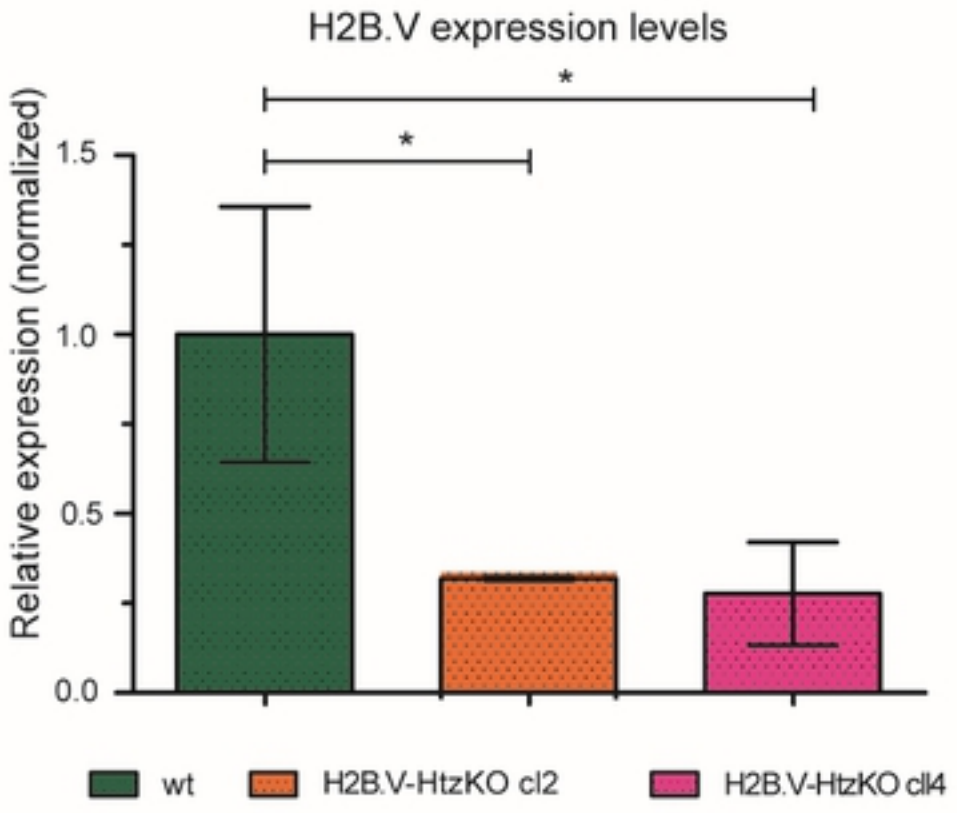

B.

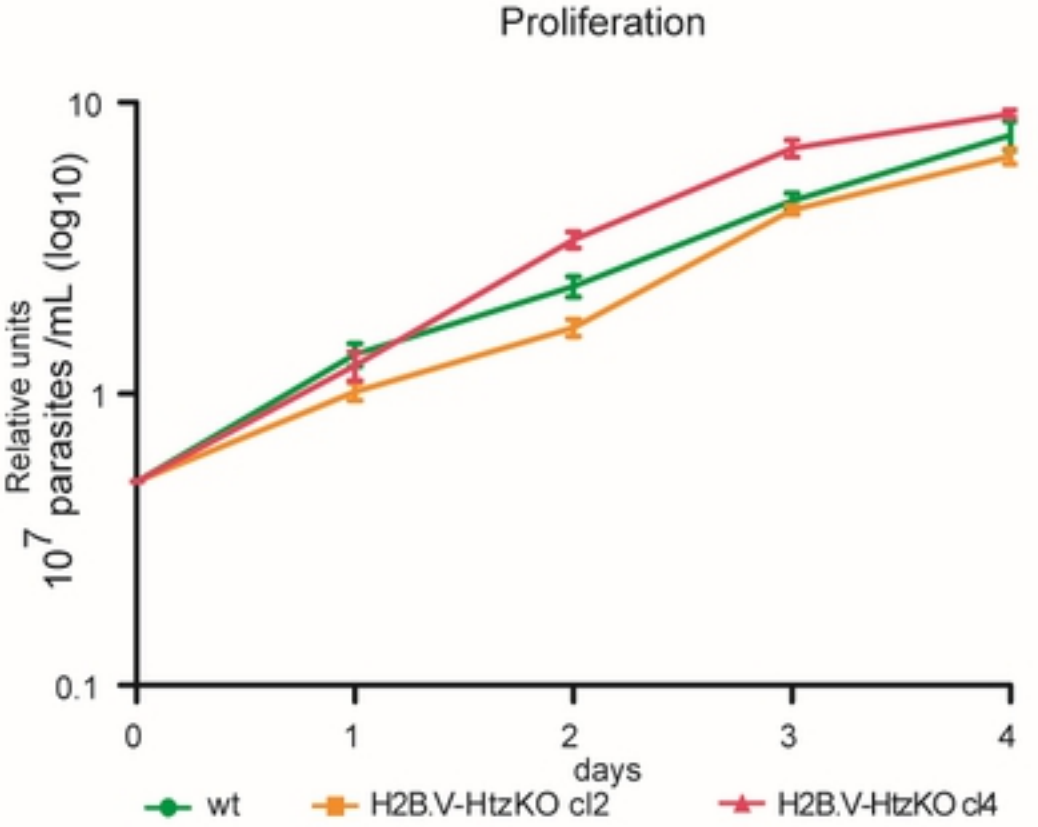

C.

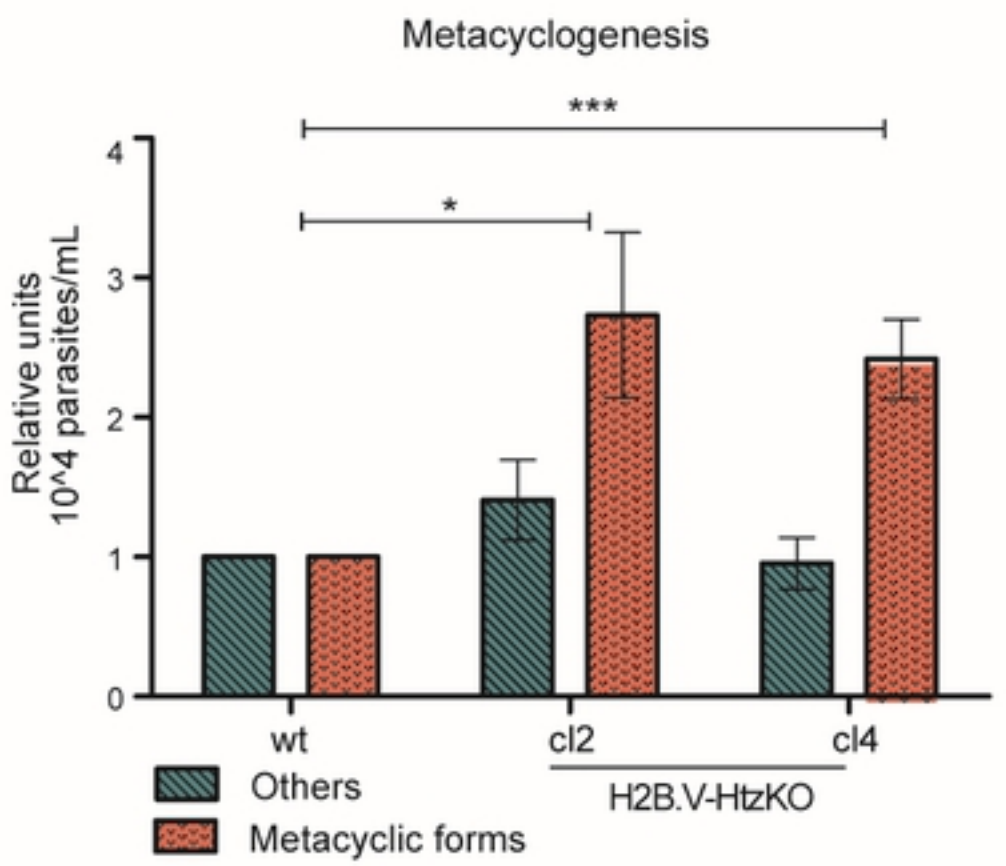

D.

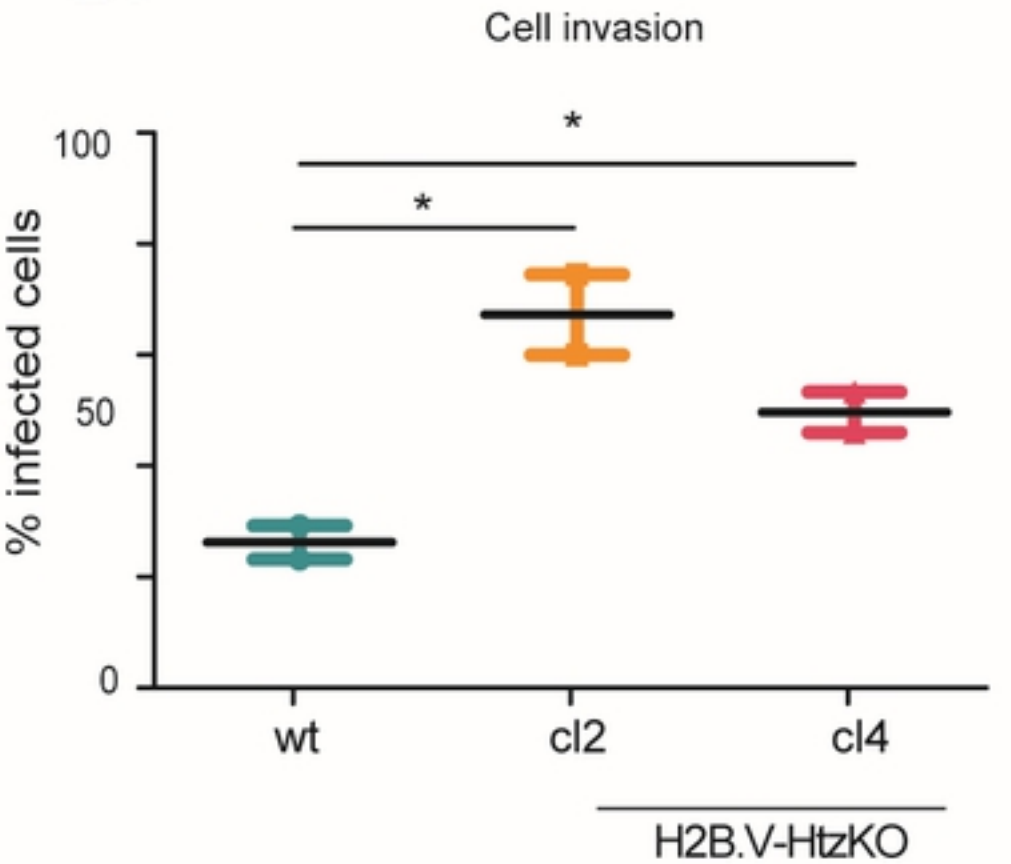

Fig4